Journal of Autoimmunity 153 (2025) 103422

Contents lists available at ScienceDirect

Journal of Autoimmunity

journal homepage: www.elsevier.com/locate/jautimm

miR-143-3p boosts extracellular vesicles to improve the dermal fibrosis of localized scleroderma

Jiahui Jin [a,b,1], Zhe Wang [a,c,1], Yifan Liu [a], Jie Chen [a], Miao Jiang [a], Lixia Lu [a], Jingying Xu [a], Furong Gao [a], Juan Wang [a], Jieping Zhang [a], Guo-Tong Xu [a], Caixia Jin [a,****], Haibin Tian [a,***], Jingjun Zhao [b,**], Qingjian Ou [a,*,2]

[a] Department of Dermatology and Laboratory of Clinical and Visual Sciences, Tongji Hospital, School of Medicine, Tongji University, Shanghai, China
[b] Department of Dermatology, Xinhua Hospital Affiliated to Shanghai Jiao Tong University School of Medicine, Shanghai, China
[c] Department of Physiology, College of Basic Medical Sciences, Naval Medical University, Shanghai, China

ARTICLE INFO

Handling editor: C Selmi

Keywords:
Localized scleroderma
Dermal fibrosis
miR-143-3p
Bone marrow mesenchymal stem cell
Extracellular vesicles

ABSTRACT

Localized scleroderma (LoSc) is an autoimmune disease that features extensive fibrosis of the skin. Due to its severity and limited understanding, no effective treatments have been developed to date. Bone marrow mesenchymal stem cells (BMSCs) derived extracellular vesicles (EVs) have been demonstrated promising therapeutic effects on the LoSc mouse model in our previous study. However, identifying the targets and underlying mechanisms of EVs remains a significant challenge for therapeutic applications. miR-143-3p, a critical and abundant factor in BMSC-EVs identified through miRNA sequencing, mediates antifibrotic effects in a LoSc mouse model and is significantly lacking in the dermis of LoSc patients. This microRNA inhibits myofibroblast formation and collagen synthesis, contributing to the therapeutic effects of BMSC-EVs in the LoSc mouse model. Moreover, miR-143-3p-reinforced BMSC-EVs demonstrated enhanced therapeutic efficacy compared to normal BMSC-EVs, reducing dermal thickening, collagen deposition, fibroblast differentiation into myofibroblasts, and promoting skin tissue remodeling. IGF1R, highly expressed in the skin of LoSc, was identified as a potential target of miR-143-3p and was inhibited by miR-143-3p-reinforced EVs, thereby modulating the IGF1/IGF1R-AKT/MAPK pathway. In conclusion, miR-143-3p-enriched EVs could be a more efficient candidate for treating dermal fibrosis in LoSc.

1. Introduction

Scleroderma, including localized scleroderma (LoSc) and systemic sclerosis (SSc), is an autoimmune and fibrotic connective tissue disease that has been linked to continuous activation of fibroblasts towards myofibroblasts and excessive deposition of extracellular matrix (ECM) [1,2]. SSc is a complex multisystem autoimmune disorder marked by widespread microvascular damage, immune dysregulation, and excessive collagen deposition, affecting the skin, blood vessels, and various visceral organs. In contrast, LoSc is primarily confined to the skin and subcutaneous tissues, presenting with inflammation and fibrosis but lacking systemic involvement. The clinical manifestations of LoSc are divided into active and inactive lesions. The active lesions show an inflammatory phase characterized by congestion and edema, and a progressive fibrosis phase, whereas the inactive lesions exhibit the phase of atrophic or scarring [3,4]. LoSc and SSc currently have no curative treatment due to the limited knowledge of complex pathogenic mechanisms.

Generally, the differentiation of fibroblasts or epithelial cells into myofibroblasts and the persistence of myofibroblasts are considered key characteristics of pathological fibrosis and scleroderma [5,6]. Exposure of the myofibroblasts to a dysregulated extracellular environment and

* Corresponding author.
** Corresponding author.
*** Corresponding author.
**** Corresponding author.
E-mail addresses: jincx@tongji.edu.cn (C. Jin), tianhb@tongji.edu.cn (H. Tian), zhaojingjun2015@aliyun.com (J. Zhao), vip@ouqingjian.com (Q. Ou).
[1] J. Jin and Z. Wang contributed equally to this paper.
[2] Lead contact.

https://doi.org/10.1016/j.jaut.2025.103422
Received 10 May 2024; Received in revised form 15 March 2025; Accepted 14 April 2025
Available online 23 April 2025

abnormal ECM cues can lead to further collagen deposition and dermal fibrosis [7,8]. Several have proposed that preventing the development of myofibroblasts may be a useful strategy to retard the fibrotic process or perhaps halt or reverse existing fibrosis. Therefore, inhibiting the differentiation and survival of myofibroblasts has been the critical target for treatment of scleroderma [9,10].

Several miRNAs, like miR-23a, miR-155, miR-29a, and so on, have been reported to be helpful in fibrotic diseases by targeting specific mRNAs and, as a result, proteins in target cells to improve fibrosis. And let-7a, miR-7, miR-196a, miR-155, miR-483-5p, and miR-29a are molecules that influence the production and deposition of the ECM [11–13]. In addition, extracellular vesicles (EVs) are ideal drug delivery methods because they can transport and preserve nucleic acids, traverse biological barriers, and target cells [14]. For many cell types, intracellular transport of EVs has been proven, and this enables the effective delivery of miRNAs, which also serve as a major functional component of EVs and are thought to play a significant role in their therapeutic action [15]. Therefore, we also pay special attention to investigating effective miRNAs that are abundantly expressed in EVs and pathologically reduced in LoSc mouse model or patients. We consider that critical and therapeutic miRNAs can be loaded into EVs in artificially high abundance to achieve better therapeutic efficacy of LoSc.

Transplantation of multiple sources of mesenchymal stem cells (MSC) has garnered significant attention as a potential approach for treating tissue regeneration and autoimmune diseases, including scleroderma [16]. Additionally, stem cell-derived EVs comprise an essential component of intercellular exchange and have pleiotropic functions [17]. MSCs-EVs, major paracrine factors and delivery vectors, have been considered an attractive candidate and substantial alternative to stem cell-based therapy in LoSc and SSc. In our previous study, topical injection of BMSC or BMSCs-EVs are confirmed to reduce skin fibrosis and ROS-induced apoptosis in the bleomycin (BLM) induced mouse LoSc model [18–20]. Thus, the detailed components and mechanisms, including the nucleic acids of BMSC-derived EVs, warrant further investigation.

In continuation of our previous study, we carried out miRNA sequencing of BMSC-EVs and identified the critical and functional miRNAs of BMSC-EVs in the present study. miR-143-3p is decreased in clinical skin tissue of patients with LoSc and the mouse LoSc model. The BMSC-EVs with miR-143-3p reinforcement are confirmed to exert better effects than normal EVs, relieving ECM deposition, fibroblast differentiation into myofibroblasts, and epithelial cell activation in the epidermis by regulating the IGF1/IGF1R-AKT/MAPK signaling pathway. Our findings provide a novel and miRNA-modified EV delivery system for patients with LoSc and a miRNA biomarker for the diagnosis of scleroderma.

2. Methods

2.1. Ethics statement

For human ethics, the experiments were performed according to the guidelines and approval of the human research ethics committee of the Tongji Hospital of Tongji University (Approval No. K-2023-005). A total of four donors were involved in this study. Written informed consent was obtained from each involved patient. Admission criteria for assessing patients: (1) Patients with LoSC are required to meet the classification criteria for scleroderma established by the American College of Rheumatology [21]; (2) have a stable disease and are not on steroid, anti-fibrotic, or anti-scar therapy. The localized scleroderma skin severity index (LoSSI) was used to assess disease severity for patients. The LoSSI was created to be basic, fast, and simple to score based on information acquired from a brief assessment of a patient's clinical history and dermatological examination. The LoSSI is calculated by summing 4 domain scores based on surface area score (SA), erythema (ER), skin thickness score (ST), and new lesion/lesion extension (N/E), which were scored on four scales (0–3) [22,23].

For animal experiments, the C57BL/6 mice were purchased from SLAC Laboratory Animal Co., Ltd. (Shanghai, China). All animal experiments were approved by the Animal Welfare and Ethics Committee of Tongji University and performed according to the proposal of the Institute of Laboratory Animal Resources, Tongji University (Approval No. TJAA09623101).

2.2. Analyses of single cell RNA sequencing

The expression matrix of single-cell RNA sequencing from the skin of LoSc patients and normal controls was collected from the dataset GSE195452 [24]. The merged matrix was prepared for clustering with the R package Seurat (v4.1.0), following the common pipeline. The DEGs of each celltypes were shown in Table S1. The functions of SeuratFeaturePlot, ggplot2DotPlot, and pheatmappheatmap were used to demonstrate the expression of selected genes. The interactions between clusters were determined by the R package CellChat (v1.5.0). The CellChatnetVisual_chord_cell and CellChatnetVisual_bubble were used to visualize the interactions of ligand-receptors in the IGF signaling pathway between clusters of fibroblasts and epithelial cells.

2.3. Mouse BMSCs isolation and culture

Isolation and culture of mouse BMSCs were performed according to our previous study [25]. Briefly, the BMSCs were separated from the femurs and tibias of 4-week-old mice and cultured in a cell culture plate. Then, BMSCs were grown in the medium, which included α-MEM medium (12571063, Thermo Fisher Scientific, USA), 15 % fetal bovine serum (FBS; 10091148, Thermo Fisher Scientific, USA), and 1 × penicillin-streptomycin solution (E607011, Sangon Biotech, China). The BMSCs were passaged when they reached 80 % confluence. The typical surface markers of BMSCs (P3) were analyzed by flow cytometry.

2.4. Isolation and identification of mouse BMSCs-derived EVs

The BMSC-derived EVs were isolated from the supernatants of BMSCs by ultracentrifugation, as in our previous study [25,26]. When the mouse BMSCs reached 80 % confluence, the culture medium was replaced with α-MEM supplemented with 5 % EV-depleted FBS. The cell supernatants were collected 48 h later and centrifuged at 300 g for 10 min to remove cell pellets. Then, the supernatants were centrifuged at 2000 g for 20 min and at 10,000 g for 30 min, and then filtered through a 0.22-μm sterilized filter (GSWP04700, Merck, Germany). Next, the filtered supernatants were ultracentrifuged at 150,000 g for 2 h to isolate the EVs. The pellet of EVs was suspended in PBS (phosphate buffered saline) and re-ultracentrifuged again at 150,000 g for 2 h. Finally, the pellet was resuspended in ice-cold PBS.

For the identification and detection of extracellular vesicles, the protein concentration of EVs was measured with the BCA protein assay kit (23227, Thermo Fisher Scientific, USA). Transmission electron microscopy (TEM; Tecnai 12, FEI, USA) was used to observe the morphology of BMSC-EVs. The particle size of EVs was measured with a NanoSight NS300 instrument (Malvern Instruments, UK). In addition, the typical markers of EVs were identified by western blot.

2.5. Isolation and culture of mouse fibroblast

Mouse skin fibroblasts were isolated from the skin of embryonic mice at the 18-day gestation period with the trypsin-EDTA solution (25300062, Thermo Fisher Scientific, USA) and cultured in DMEM (D0819, Sigma Aldrich, Germany) with 10 % FBS. The fibroblasts in passage 3 were assigned for cellular assays.

2.6. Establishment and treatment of the mouse LoSc model

To establish the murine LoSc model, the mice had their backs shaved, followed by daily subcutaneous injections of 100 μL of BLM solution (1 mg/mL, R25001, Thermo Fisher Scientific, USA) into the shaved area (1 cm^2) for four weeks. After that, the LoSc mice were randomly assigned into groups and underwent the therapies listed below by subcutaneous injection of each BMSC-EV. For the EVs-miR-NC or EVs-miR-143-3p groups, the LoSc mice were treated with PBS (100 μL), EVs-miR-NC (150 μg/100 μL), or EVs-miR-143-3p (150 μg/100 μL), respectively. The mice were euthanized two weeks after the therapy with BMSC-EVs, and the skin samples were collected from a 1 cm^2 shaved area for subsequent analyses.

2.7. Transfection of miRNA mimics and inhibitors

The mouse skin fibroblasts were grown in cell culture plates and incubated until the confluence reached 60–70 %. Then, the mouse fibroblasts were transfected with the miR-21a-5p mimic (5′-UAGCUUAUCAGACUGAUGUUGA-3′)/miR-21a-5p inhibitor (5′-AACAUCAGUCUGAUAAGCUAUU-3’), the miR-143-3p mimic (5′-UGAGAUGAAGCACUGUAGCUC-3′)/miR-143-3p inhibitor (5′-GAGCUACAGUGCUUCAUCUCA-3′), and the control mimic and inhibitor (RiboBio, China) at a dose of 20 nM using lipofectamine 3000 (L3000001, Thermo Fisher Scientific, USA) for 8 h. Fresh serum-free media was added, and the cells were cultivated for an additional 48 h. Eventually, cells were gathered for RT-PCR and western blot analysis. All the cell experiments were repeated three times.

2.8. Lentiviral transduction of mouse BMSCs

To construct mouse BMSCs with stably high/low expression of miR-143-3p, the lentivirus system was applied as a modified routine in this study [27]. Briefly, the lentiviruses expressing miR-143-3p, miR-143-3p inhibitor, and control were produced from 293T with the lentiviral system. The mouse BMSCs were incubated with miR-143-3p modified or control lentiviruses, respectively, for 24 h and replaced with fresh medium for another 48 h. The positive cells were screened with puromycin (5 μg/mL; T2219, TargetMol, USA) for 24 h. Next, the level of miR-143-3p in the BMSC and BMSC-EVs was determined with RT-PCR.

2.9. Histology and immunohistochemistry (IHC) analysis

The skin tissues were fixed with 4 % paraformaldehyde (E672002, Sangon Biotech, China) solution and embedded in paraffin and analyzed as in our previous study [25]. Briefly, the paraffin-embedded sections were deparaffinized using xylene and decreasing concentrations of ethanol. Next, the tissue sections were processed with hematoxylin and eosin staining.

To detect the degree of skin fibrosis, randomly chosen portions of the skin tissue sections were involved to measure dermal thickness and subcutaneous adipose layer using ImageJ software (NIH, USA). For the collagen analysis, the sections were stained with Masson’s trichrome staining (BPDL023, SenBeiJia Biological Technology Co., Ltd, China), and the distribution of collagen fibers was observed by a microscope (Olympus, Japan).

The deparaffinized skin tissue sections were blocked with 5 % goat serum (Sangon Biotech, China) for 1 h at room temperature and treated with primary antibodies overnight at 4 °C (Table S2). Then, skin tissue sections were incubated with the corresponding secondary antibodies for 30 min at room temperature and visualized with diaminobenzidine (DAB) solution under a microscope (Olympus, Japan).

2.10. Hydroxyproline measurement

The collagen content of skin tissue in different groups was measured with the hydroxyproline test kit (A030-2-1, JianCheng Bioengineering, Nanjing, China). The hydroxyproline content of skin samples was determined from the OD values (550 nm, iMark Microplate Absorbance Reader, Bio-Rad, USA) using the formula below: (tested OD value - blank OD value)/(standard OD value - blank OD value) × standard sample concentration (5 μg/mL) × total hydrolysate volume (10 mL)/tissue wet weight (mg).

2.11. Immunofluorescence

For cellular immunofluorescence, the cell slides were washed with PBS and fixed with 4 % paraformaldehyde. The fixed cells were permeabilized with 0.03 % Triton X-100 (A600198, Sangon Biotech, China) and then blocked with 5 % goat serum (Sangon Biotech, China) for 1 h. The cell slides were incubated with primary antibodies and secondary antibodies (Table S2). The nuclear was stained with DAPI Stain Solution (E607303, Sangon Biotech, China). The representative images were acquired using a fluorescence microscope (Olympus, Tokyo, Japan).

2.12. In situ hybridization (ISH)

The enhanced sensitive ISH detection kit (Bosterbio, Wuhan, China) was applied to exactly localize the expression of miR-143-3p in skin tissue of mouse and human. The deparaffinized sections of skin tissue were digested in 3 % citric acid-diluted pepsin for 30 min at 37 °C and hybridized with the digoxin-labeled miR-143-3p probe (Sangon Biotech, China). After hybridization, the skin tissue sections were washed and blocked in a blocking solution for 30 min at 37 °C. The alkaline phosphatase-labeled mouse anti-digoxigenin was used to link the positive signals of miR-143-3p of the sections. Finally, 5-Bromo-4-Chloro-3-Indolyl Phosphate (BCIP)/Nitro-Blue-Tetrazolium (NBT) were applied to visualize the positive signal of miR-143-3p. The representative images were acquired using a microscope (Olympus, Tokyo, Japan).

2.13. Western blot assay

The skin tissues, cell samples, and BMSC-EVs were lysed in the RIPA buffer (TargetMol, USA) with protease and phosphatase inhibitors (C0001 and C0004, TargetMol, USA) to obtain total proteins. Next, the total protein was separated with 10 % SDS-PAGE and transferred to PVDF membranes (IPFL85R, Merck, Germany). The blotted membrane was blocked with 5 % BSA (A600903, Sangon Biotech, China) and incubated with the primary antibodies and HRP-conjugated secondary antibodies (Table S2). Finally, the images of target protein bands were visualized using the ECL Western blotting substrate (32209, Thermo Fisher Scientific, USA) with the Tanon chemiluminescence image detection system (5200S, Tanon, China).

2.14. RNA extraction and quantitative real-time PCR

The total RNA of cells, skin tissues, and BMSC-EVs was extracted using TRIzol reagent (9109, Takara, Japan), and cDNA was obtained by PrimeScript RT Master Mix (RR036A, Takara, Japan). Quantitative real-time PCR was analyzed using SYBR Green Realtime PCR Master Mix (FP205-03, Tiangen, China) under the manufacturer’s instructions. For the detection of the relative expression of miRNA, miRcute Plus miRNA First-Strand cDNA Kit (KR211-01, Tiangen, China) was utilized to reverse transcribe the cDNA, and quantitative real-time PCR was performed by the miRcute Plus miRNA qPCR Kit (FP411, Tiangen, China). The primers (Sangon Biotech, China) used for our study are shown in Table S3. The expression of detected gene was analyzed using the $2^{-\Delta\Delta Ct}$ method with normalization to the average expression of GAPDH (tissue and cell) or U6 (miRNA).

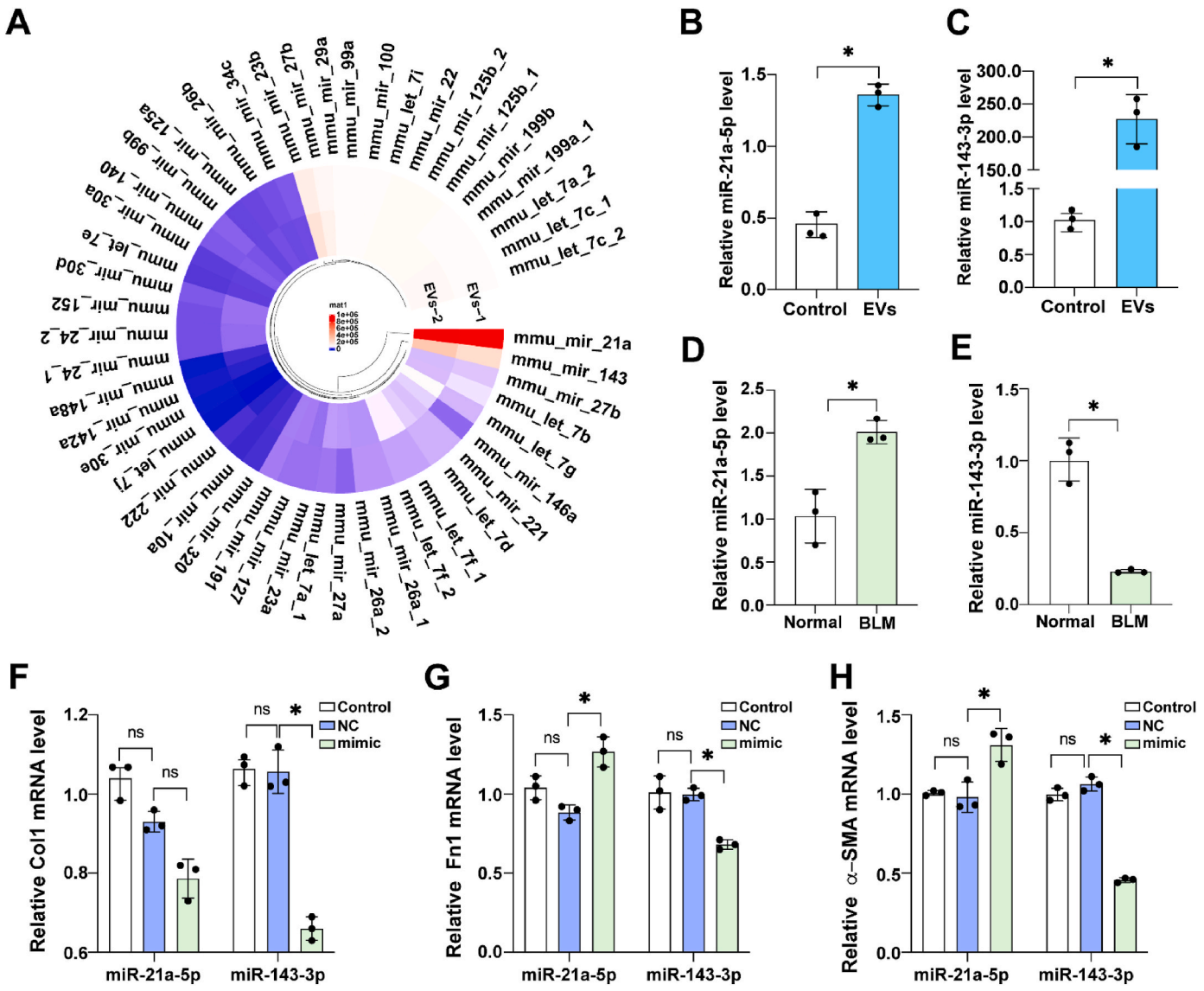

Fig. 1. Identification of miR-143-3p as a key BMSC-EVs component for the treatment of scleroderma.
(A) miRNA profile analysis of mouse BMSC-EVs by high-throughput small RNA sequencing. The relative expression levels of highly expressed miRNAs in mouse BMSC-EVs were shown by a heatmap. **(B–C)** RT-PCR analysis of the top 2 miRNAs in BMSC-EVs-treated mouse fibroblasts; PBS-treated fibroblasts served as controls (n = 3). **(D–E)** RT-PCR analyzed the expression of a miR-21a-5p and miR-143-3p in skin tissues of bleomycin (BLM) induced mouse LoSc model after BMSC-EVs treatment (n = 3). **(F–H)** RT-PCR analysis of mRNA expression of *Col1*, *Fn1*, and *α-SMA* in fibroblasts treated with the 2 miRNA mimics (miR-21a-5p, miR-143-3p) or control mimics (miR-NC) (n = 3). Data are presented as mean ± SD; *, P < 0.05.

2.15. Data preprocessing and screening of DEGs

The gene expression matrix of GSE165117 was downloaded and examined using the limma package. DEGs have to meet the screening requirements of |log fold change (log FC)| > 1 and an adjusted p-value of 0.05. The p-value was adjusted using the false discovery rate (FDR). The target genes of miRNA-143-3p were predicted by several target gene prediction programs, consisting of TargetScan (https://www.targetscan.org/vert_80/), miRDB (http://mirdb.org/), starBase (http://starbase.sysu.edu.cn/), and ENCORI (https://rnasysu.com/encori/). Only the 4 predicted mRNAs that appeared in these four programs were included for subsequent analyses.

2.16. Dual-luciferase reporter gene assay

The 3′ untranslated regions (UTR) of Igf1r were PCR-amplified from mouse genomic DNA, and primer sequences are as follows: Forward, 5′-TCTAGGCGATCGCTCGAGGTTTTAATCACTGTAGAAAAGC-3’; Reverse, 5′- TTGCGGCCAGCGGCCGCTGTAGGGGACCAGGTGAGGAGAA-3’. Then, the complete Igf1r 3′UTR was cloned into the psiCHECK-2 vector (Promega, USA) as the wild-type (WT) by the ready-to-use seamless cloning kit (B632219, Sangon, China). Then, the mutant type vectors (MT) containing the mutations corresponding to the miR-143-3p binding target in the 3′UTR of Igf1r were synthesized and cloned with the seamless cloning kit. The WT or MT constructs were transfected separately and co-transfected with NC-mimic or miR-143-3p mimics into 293T cells using lipofectamine 3000 (Thermo Fisher Scientific, USA). After 48 h, the Renilla-Firefly luciferase activity was determined using a dual luciferase reporter gene assay kit (11401ES76, Yeasen, China) according to the manufacturer’s instructions.

2.17. Analyses of bulk RNA sequencing

To explore the expressions of IGF1 and IGF1R in LoSc patients and

normal controls, we analyzed the bulk RNA sequencing dataset from GSE166861 and GSE166863 [28,29]. The trim_galore software (v0.6.10) was used to trim adapters of FastQ files that were downloaded from the Sequence Read Archive (SRA). The cleaned RNA-seq reads were aligned to hg38 with STAR (v2.7.11a). Then the gene counts were derived from the number of uniquely aligned, unambiguous reads by the software Subread:featureCount (v2.0.6). The expression matrix was analyzed with the R package limma (v3.52.4) following the pipelines in Ritchie et al. [30]. The R package ggplot2 (v3.4.3) was used to visualize the expressions of *IGF1* and *IGF1R*.

2.18. Statistical analysis

All data were analyzed using GraphPad Prism software (version 9.0, USA). The unpaired Student's t-test was used to compare data between two groups. One-way analysis of variance (ANOVA) was performed for the comparisons of multiple groups. All data are shown as mean ± standard deviation (SD). Results were considered statistically significant at p-value <0.05.

3. Results

3.1. miR-143-3p functioned as a critical effector in BMSC-EVs mediated antifibrotic effects

To screen the functional miRNAs of BMSC-EVs that can cure scleroderma, as confirmed in our previous study, the mouse BMSC-EVs were identified through miRNA sequencing and deposited in the NCBI GEO database (GSE164965) [25]. As shown in Fig. 1A, the top 2 abundant miRNAs of the mouse BMSC-EVs were miR-21a-5p and miR-143-3p, according to the miRNA-seq. Furthermore, the expression levels of the 2 miRNAs were evaluated in mouse skin fibroblast cells that were treated with the BMSC-EVs for 48 h. The results showed that the levels of miR-21a-5p and miR-143-3p in the BMSC-EVs group were significantly increased compared with those in the control (PBS) treated group, confirming the ability of BMSC-EVs to transport their contained miRNAs into fibroblasts (Fig. 1B and C). Notably, the expression of miR-143-3p in the BMSC-EVs treatment group was more than 200 times higher than that of the control group. Meanwhile, we detected the levels of miR-21a-5p and miR-143-3p in the skin tissues of the BLM induced LoSc mouse model. miR-143-3p was significantly decreased in the LoSc mouse model compared to normal control mice, while this level of miR-21a-5p was increased in the mouse LoSc model (Fig. 1D and E).

To investigate the cellular function of these 2 miRNAs on skin fibroblasts, the 2 miRNA mimics were transfected into fibroblasts of mice in vitro, respectively. The expression of pro-fibrotic markers (*Col1, Fn1,* and *α-SMA*) in skin fibroblasts was evaluated with RT-PCR assays. The results revealed that miR-143-3p significantly suppressed the mRNA expression of *Col1* (P = 0.0231), *Fn1* (P = 0.0259), and *α-SMA* (P = 0.0328) in fibroblasts (Fig. 1F–H). In addition, miR-21a-5p did not inhibit the expression of pro-fibrotic markers (*Col1, Fn1, α-SMA*) in fibroblasts. These results suggested that miR-143-3p, which was abundant in BMSC-EVs, played an essential part in inhibiting the trans-differentiation of fibroblasts to myofibroblasts and the synthesis of collagen in fibroblasts.

3.2. The expression of miR-143-3p is downregulated in the patients with LoSc

Since miR-143-3p is highly necessary for BMSC-EVs to treat the mouse LoSc model and the sequences for hsa-miR-143-3p (UGAGAUGAAGCACUGUAGCUC; miRBase database) and mmu-miR-143-3p (UGAGAUGAAGCACUGUAGCUC; miRBase database) are identical, we therefore asked whether the expression of miR-143-3p in the skin tissues of patients diagnosed with LoSc was decreased or not. Four patients diagnosed as LoSc according to the current diagnostic approach were recruited (Table 1) [31]. Both active and inactive LoSc lesions were included in this study. As shown in Fig. 2A, patient 1 shows active lesions, which have a white and waxy distribution area, while patient 2 shows chronic damage features, which show a raised waxy center with moderate to severe skin thickening and hyperpigmentation changes in the waxy center.

Table 1
The characteristic of LoSc patients.

	Age	Sex	Course (month)	Site of Specimen	LoS-SI
1	29	Female	12	Back	3
2	5	Male	6	Right lower abdomen	4
3	4	Female	6	Right thigh	2
4	5	Male	8	Forehead	3

Next, analysis of morphology and collagen deposition was performed on lesional punch biopsy specimens to confirm the characteristics of LoSc. Both types of LoSc showed typical thickening of the dermis layer (Fig. 2B) and collagen deposition (Fig. 2C). Moreover, RT-PCR revealed that levels of α-SMA increased by about 2-fold compared to normal skin tissue. (Fig. 2D). The expression of miR-143-3p in human LoSc tissue was also investigated. miR-143-3p was significantly decreased in the dermal layer of LoSc, as shown by RT-PCR (Fig. 2E). The histopathology analysis showed extensive expression of α-SMA in the dermis of the mouse LoSc model and the skin of LoSc patients (Fig. 2F). In situ hybridization of skin tissue showed that a positive signal for miR-143-3p was evident in normal dermal fibroblasts but not in the fibroblasts of LoSc, which is consistent with the results of RT-PCR (Fig. 2G). Thus, we inferred that miR-143-3p is necessary for maintaining skin homeostasis and should be an important complementary factor in improving scleroderma.

3.3. miR-143-3p inhibited myofibroblast formation and the synthesis of collagen in mouse fibroblasts

We next sought to investigate whether miR-143-3p can regulate the formation of myofibroblasts and the synthesis of collagen in fibroblasts of mouse skin, which are considered a cell-based model of fibrosis study [32]. Firstly, miR-143-3p mimics or inhibitors were applied to increase or decrease the levels of miR-143-3p in the fibroblasts. As shown in Fig. 3A and B, fibroblasts transfected with miR-143-3p mimics had considerably lower relative protein levels of α-SMA compared to control mimics. Consistently, inhibition of miR-143-3p with an inhibitor significantly increases the expression of α-SMA. Moreover, the non-stress fiber was significantly decreased with the overexpression of miR-143-3p, while inhibition of miR-143-3p promoted the formation of the stress fiber of α-SMA (Fig. 3C and D).

The ECM production marker Fn1 and the levels of collagens were used to analyze the activated level of myofibroblasts with these miR-143-3p increased or inhibited treatments. The expression of Fn1 was suppressed after miR-143-3p overexpression, while inhibition of miR-143-3p enhanced the protein expression of Fn1 in the mouse fibroblasts (Fig. 3E). And overexpression of miR-143-3p significantly decreased the content of hydroxyproline, a major component of the protein collagen, in fibroblasts compared with the control group, while inhibition of miR-143-3p expression did the opposite (Fig. 3F).

Returning to the issue that concerns us most, whether BMSC-EVs contain miR-143-3p is vital for BMSC-EVs to regulate myofibroblast formation and the synthesis of collagen in skin fibroblasts or not. As shown in Fig. 3G, the expression of α-SMA could be efficiently reduced by the BMSC-EVs, but administration of a miR-143-3p inhibitor rescued α-SMA expression in the fibroblasts of mouse skin. BMSC-EVs treatment also decreased the expression of ECM proteins (Fn1) and the content of collagen in fibroblasts, which were also significantly reversed by the miR-143-3p inhibitor (Fig. 3H and I).

Together, these results indicate that miR-143-3p is essential for

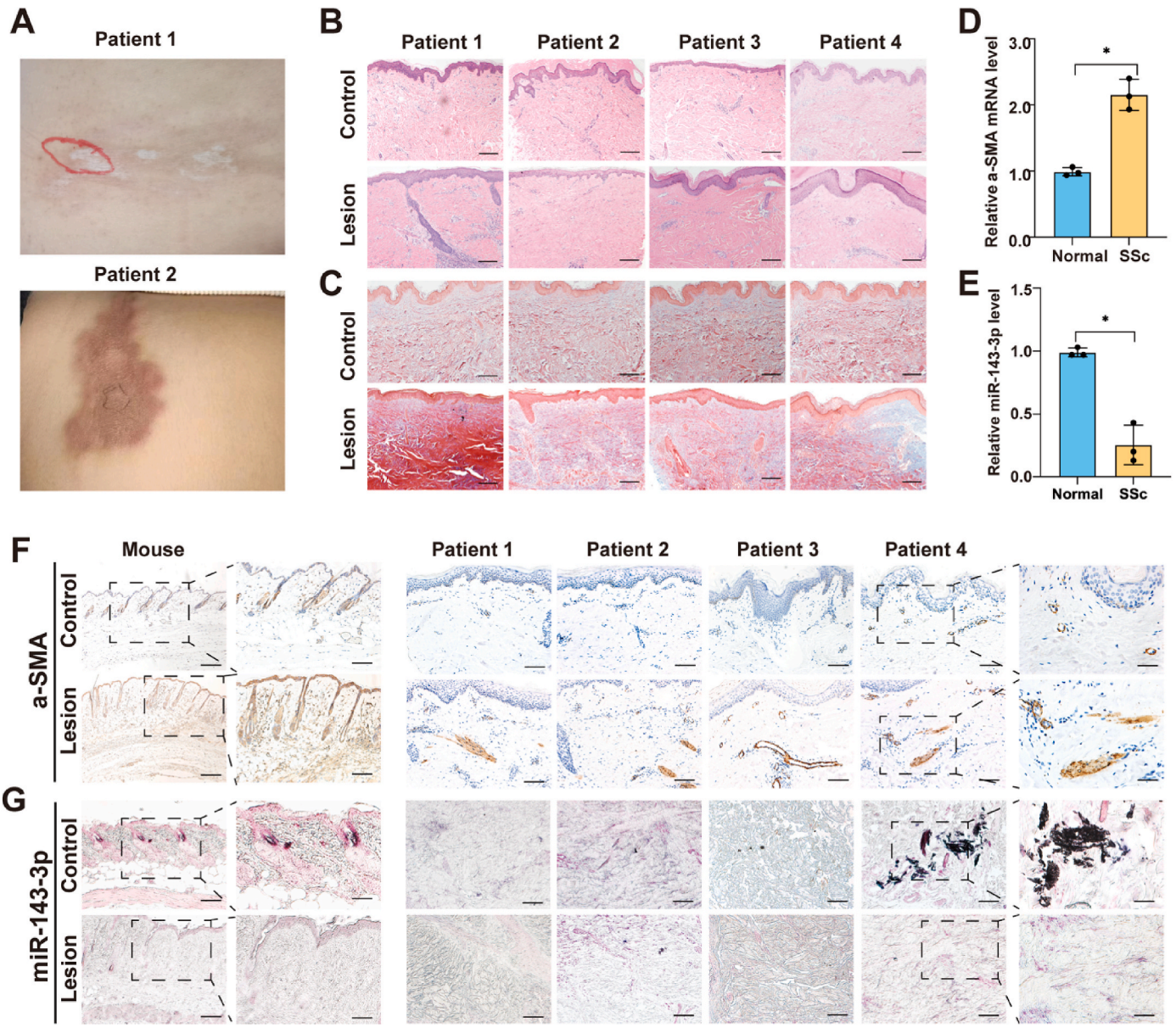

Fig. 2. miR-143-3p decreased in the dermal tissues of humans and mice with LoSc.
(A) Typical photographs of the lesions owing to localized scleroderma (LoSc) in patients. **(B)** H&E staining of representative skin sections from normal and lesion skin samples. Scale bar: 100 μm. **(C)** Masson's trichrome staining of the representative skin sections from normal and lesion skin samples. Scale bar: 100 μm. **(D–E)** Quantification of *α-SMA* (D) and miR-143-3p (E) of the representative skin sections from normal and lesion skin samples. **(F)** Representative immunohistochemical staining of α-SMA of the representative skin sections of normal and lesion skin samples from mice and patients. Scale bar: 100 μm. **(G)** In situ hybridization shows the localization of miR-143-3p in skin samples of normal and LoSc from mice and patients. Scale bar: 100 μm.

BMSC-EVs to suppress myofibroblast formation and synthesis of collagen in skin fibroblasts, as well as inhibit the fibrosis. It's necessary to enhance the expression of miR-143-3p in the BMSC to obtain the miR-143-3p enriched EVs.

3.4. Characterization of EVs derived from miR-143-3p modified mouse BMSCs

To specifically modify the contents of BMSC-EVs, we manipulated the expression of miR-143-3p in mouse BMSCs by employing lentiviral vectors containing miR-143-3p or miR-143-3p inhibitors, thereby either increasing or decreasing the level of miR-143-3p in BMSC-EVs. The characterization of EVs derived from these BMSCs is important for subsequent studies. Firstly, the transfected BMSCs show similar morphology to the control group, as seen in Fig. 4A. Next, EVs were isolated from the supernatants of each BMSC with ultracentrifugation. TEM (Transmission Electron Microscope) analysis revealed that all the EVs from the above BMSCs showed typical bilayer membrane vesicles (Fig. 4B). Additionally, the particle sizes of the EVs analyzed with NTA (Nanoparticle Tracking Analysis) showed that the particle diameters of normal EVs (mean = 137.5 nm, SD = 45.6 nm), NC-i-EVs (mean = 122 nm, SD = 34.1 nm), i-EVs (mean = 134.1 nm, SD = 43.2 nm), NC-OE-EVs (mean = 141 nm, SD = 49.6 nm), and OE-EVs (mean = 121.9 nm, SD = 33.2 nm) (Fig. 4C).

Then, the levels of miR-143-3p in both BMSC and BMSC-EVs were evaluated by RT-PCR. Firstly, compared with normal or control BMSCs, miR-143-3p of BMSCs-i was significantly decreased by approximately 50 % ($P = 0.0216$), while BMSCs-miR-143-3p overexpressed exogenous miR-143-3p genes approximately 10-fold higher than the control group ($P = 0.0062$) (Fig. 4D). For the BMSC-EVs, the miR-143-3p was also

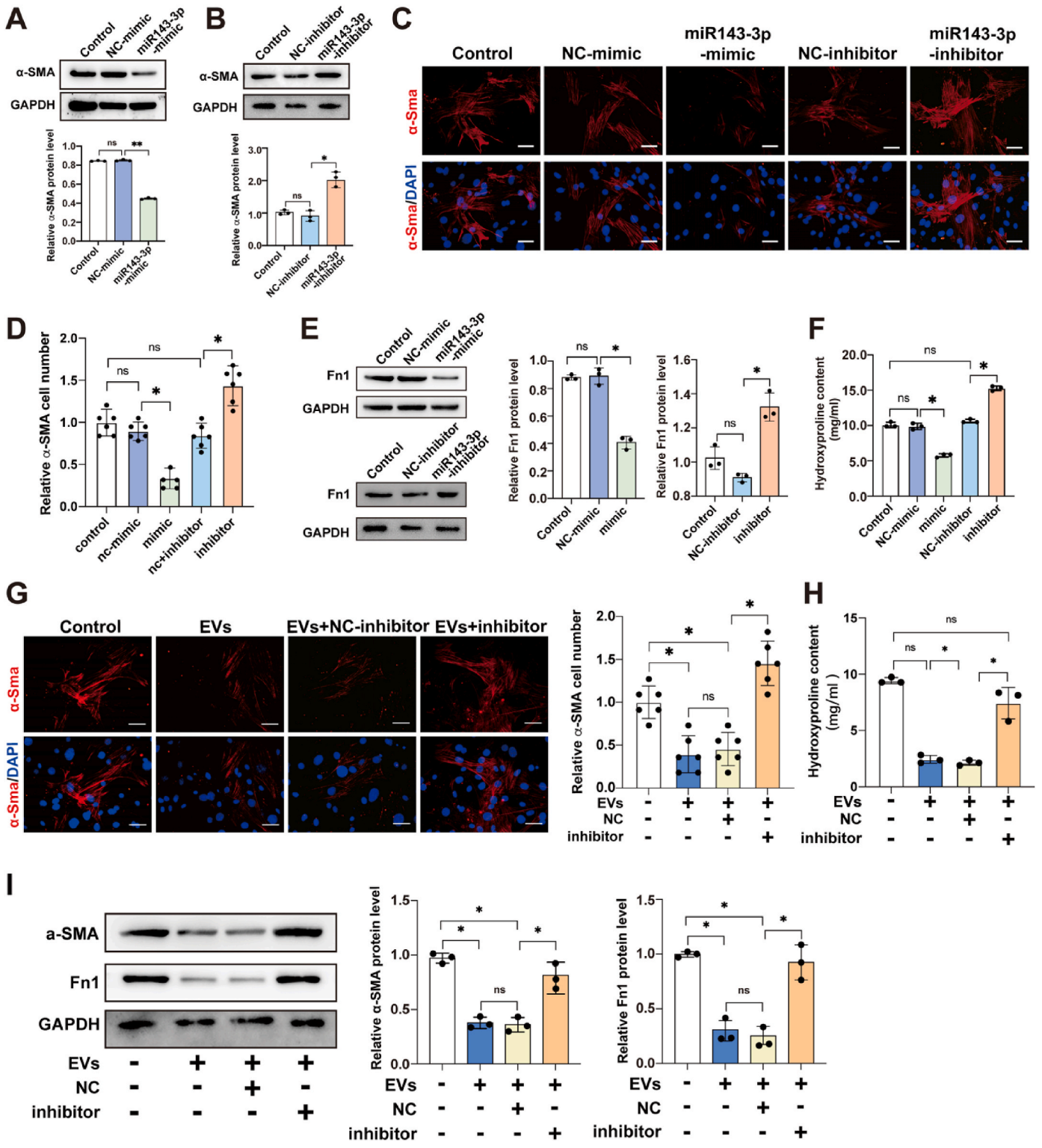

Fig. 3. miR-143-3p inhibits myofibroblast formation and the synthesis of collagen in mouse fibroblasts
(A-B) α-SMA protein expression of mouse fibroblasts with miR-143-3p overexpression (miR-143-3p mimic) or knockdown (miR-143-3p inhibitor) was detected by Western blot. **(C–D)** Immunofluorescence showing α-SMA levels and distribution of mouse fibroblasts with miR-143-3p overexpression or inhibition. Scale bar: 200 μm. **(E)** Fn1 protein expression in fibroblasts with miR-143-3p overexpression or knockdown was detected by Western blot. **(F)** The collagen contents of fibroblasts with miR-143-3p modified were quantified by hydroxyproline assay. **(G)** Immunofluorescence showing α-SMA protein expression and distribution of mouse fibroblasts treated with the BMSC-EVs or BMSC-EVs plus miR-143-3p-inhibitor. Scale bar: 200 μm. **(H)** The collagen contents of mouse fibroblasts treated with the BMSC-EVs or BMSC-EVs plus miR-143-3p-inhibitor were quantified by hydroxyproline assay. **(I)** α-SMA and Fn1 protein expression of fibroblasts treated with the BMSC-EVs or BMSC-EVs plus miR-143-3p-inhibitor were detected by Western blot. Data are presented as mean ± SD; *, $P < 0.05$; **, $P < 0.01$.

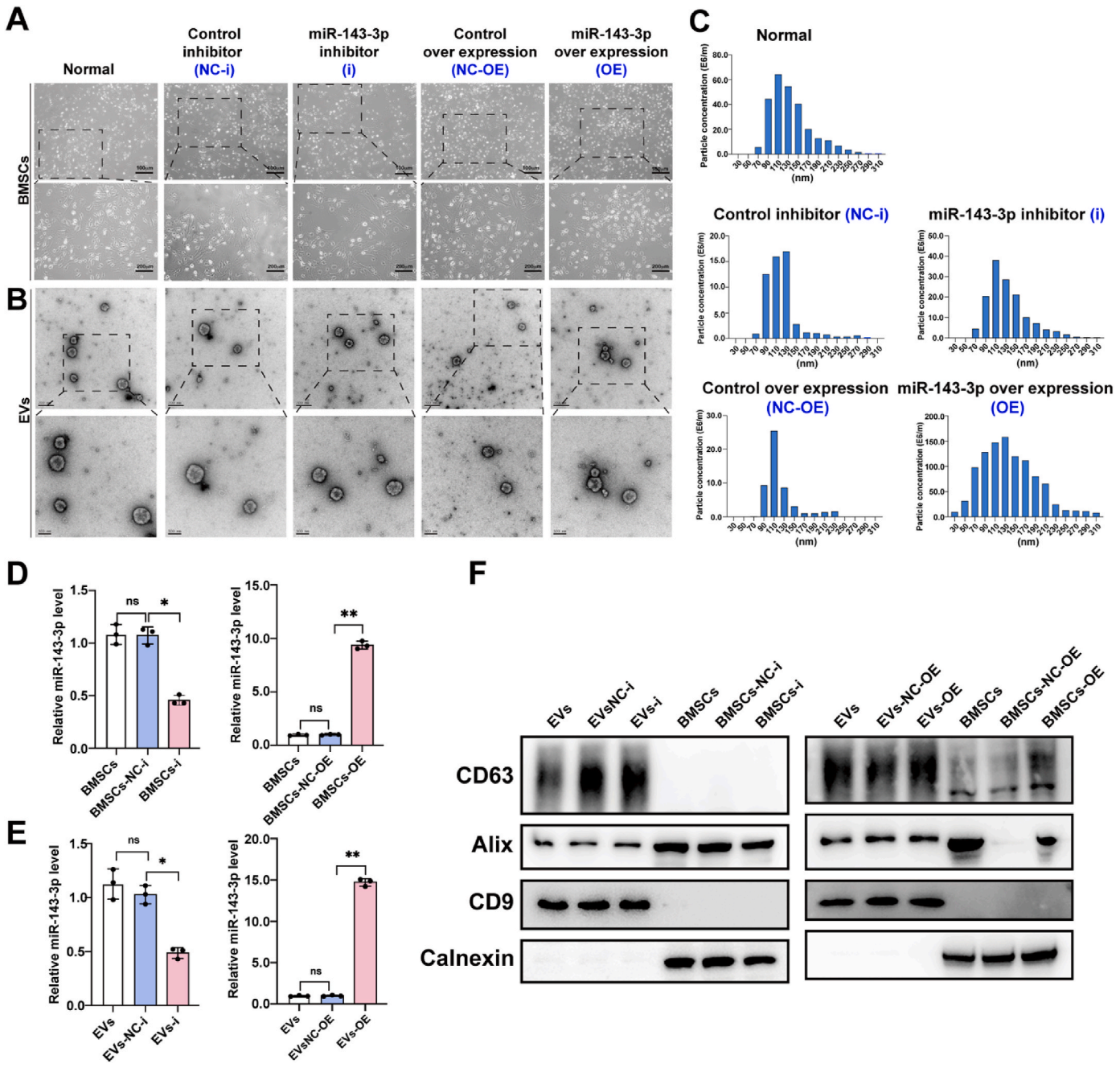

Fig. 4. Characterization of extracellular vesicles derived from modified BMSCs
(A) Morphology of BMSCs cultured in medium after various lentivirus transfections. **(B)** Morphology of normal EVs, control-inhibitor (NC-i), miR-143-3p inhibitor (i), control overexpression (NC-OE), and miR-143-3p overexpression (OE) observed by TEM. **(C)** Particle size distribution and concentration of the above five groups of EVs were measured by the NanoSight NS300 system. **(D–E)** RT-PCR was used to detect the level of miR-143-3p in BMSCs (D)/BMSC-EVs (E) with miR-143-3p modified or control. **(F)** Western blotting analysis of the surface markers of BMSC-EVs from the miR-143-3p modified BMSCs compared with cell extraction. Data are presented as mean ± SD; *, $P < 0.05$; **, $P < 0.01$.

decreased by approximately 50 %, compared to the normal or control group. Finally, the miR-143-3p levels of BMSC-EVs with miR-143-3p overexpression increase approximately 15-fold higher than the normal or control group ($P = 0.0356$) (Fig. 4E). The surface markers CD9, CD63, and ALIX were enriched in all the EVs compared to BMSCs, whereas CALNEXIN, an endoplasmic reticulum-associated protein, was not detected in these extracellular vesicles (Fig. 4F). These data lead to the conclusion that miR-143-3p-modified EVs isolated from mouse BMSCs, which were manually manipulated to increase or decrease miR-143-3p, have the typical characteristics of EVs.

3.5. miR-143-3p-reinforced EVs reduced dermal thickening and fibrosis in the mouse LoSc model

To study and evaluate the efficacy of miR-143-3p-modified BMSC-EVs on LoSc *in vivo*, we applied the above miR-143-3p modified BMSC-EVs to treat the mouse model. The mice in the LoSc model induced by BLM were subcutaneously injected with the above miR-143-3p-modified EVs. After two weeks of treatment, EVs with inhibition of miR-143-3p did not significantly improve the disease status, including the dermal thickness, did not show a recovery in the subcutaneous adipose layer, and exhibited similar thickness compared with the PBS-treated group

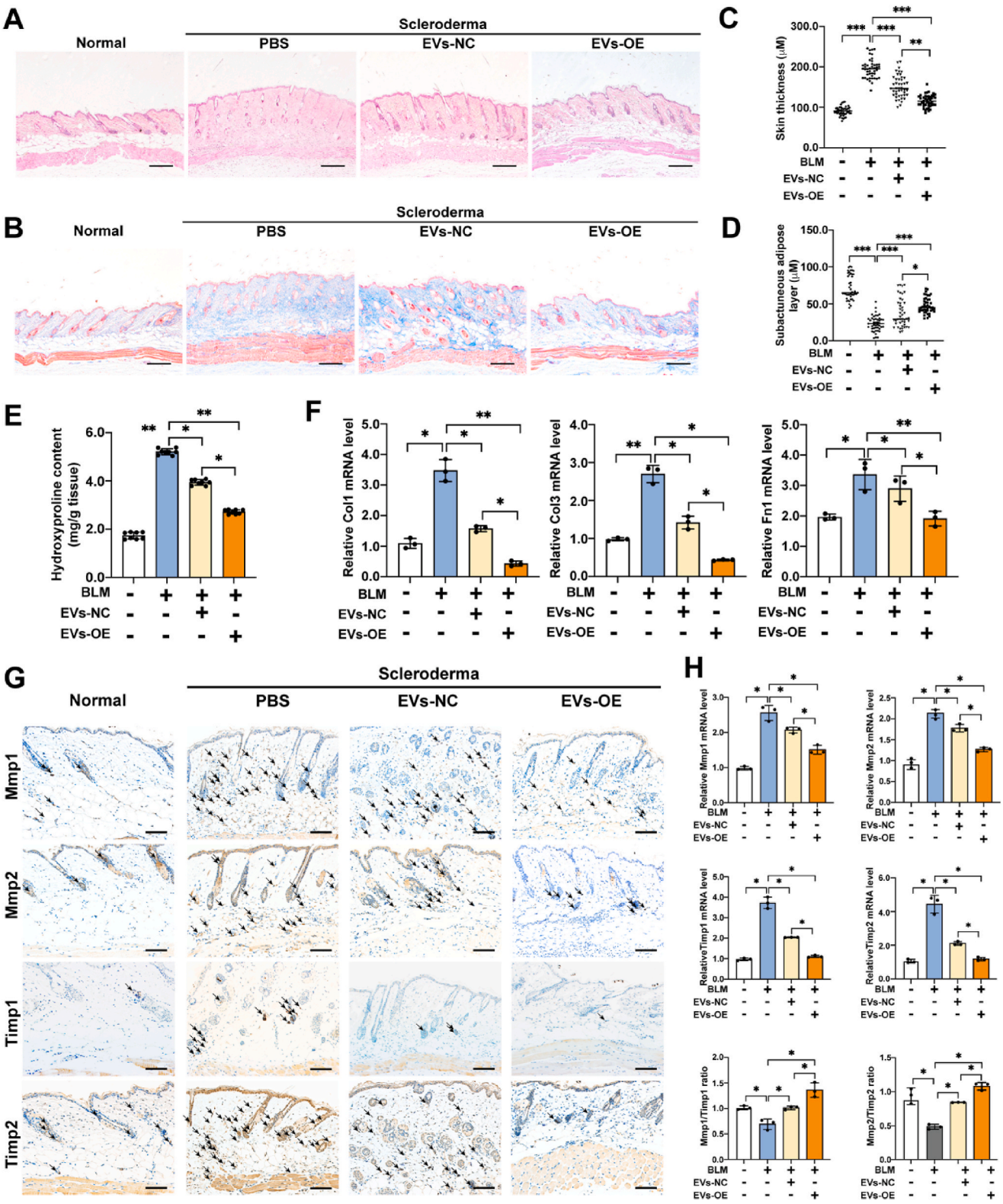

Fig. 5. miR-143-3p-modified EVs reduce dermal thickening and abnormal deposition of collagen in the mouse LoSc model.
(A) H&E staining of representative skin sections from mouse skin tissue treated with miR-143-3p modified BMSC-EVs for 14 days. Scale bar: 100 μm. **(B)** Masson's trichrome staining of the representative skin sections from mice treated with miR-143-3p-reinforced BMSC treatment or control for 14 days. Scale bar: 100 μm. **(C–D)** The thicknesses of the dermis (C) and subcutaneous fat (D) were measured from the H&E-stained dermal morphology (n = 6; 3 slides were randomly selected from each sample). **(E)** The collagen contents of dermis with miR-143-3p reinforced BMSC-EVs treatment were quantified by hydroxyproline assay (n = 8). **(F)** The expression of *Col1*, *Col3*, and *Fn1* in the skin tissues treated with miR-143-3p-reinforced BMSCs-EVs or control was quantified by RT-PCR (n = 3). **(G)** Representative immunohistochemical staining of Timp1, Timp2, Mmp1, and Mmp2. Scale bar: 200 μm. **(H)** The expression of *Timp1*, *Timp2*, *Mmp1*, and *Mmp2* in the skin tissues treated with miR-143-3p-reinforced BMSCs-EVs or control was quantified by RT-PCR (n = 3). Data are presented as mean ± SD; *, $P < 0.05$; **, $P < 0.01$; ***, $P < 0.001$.

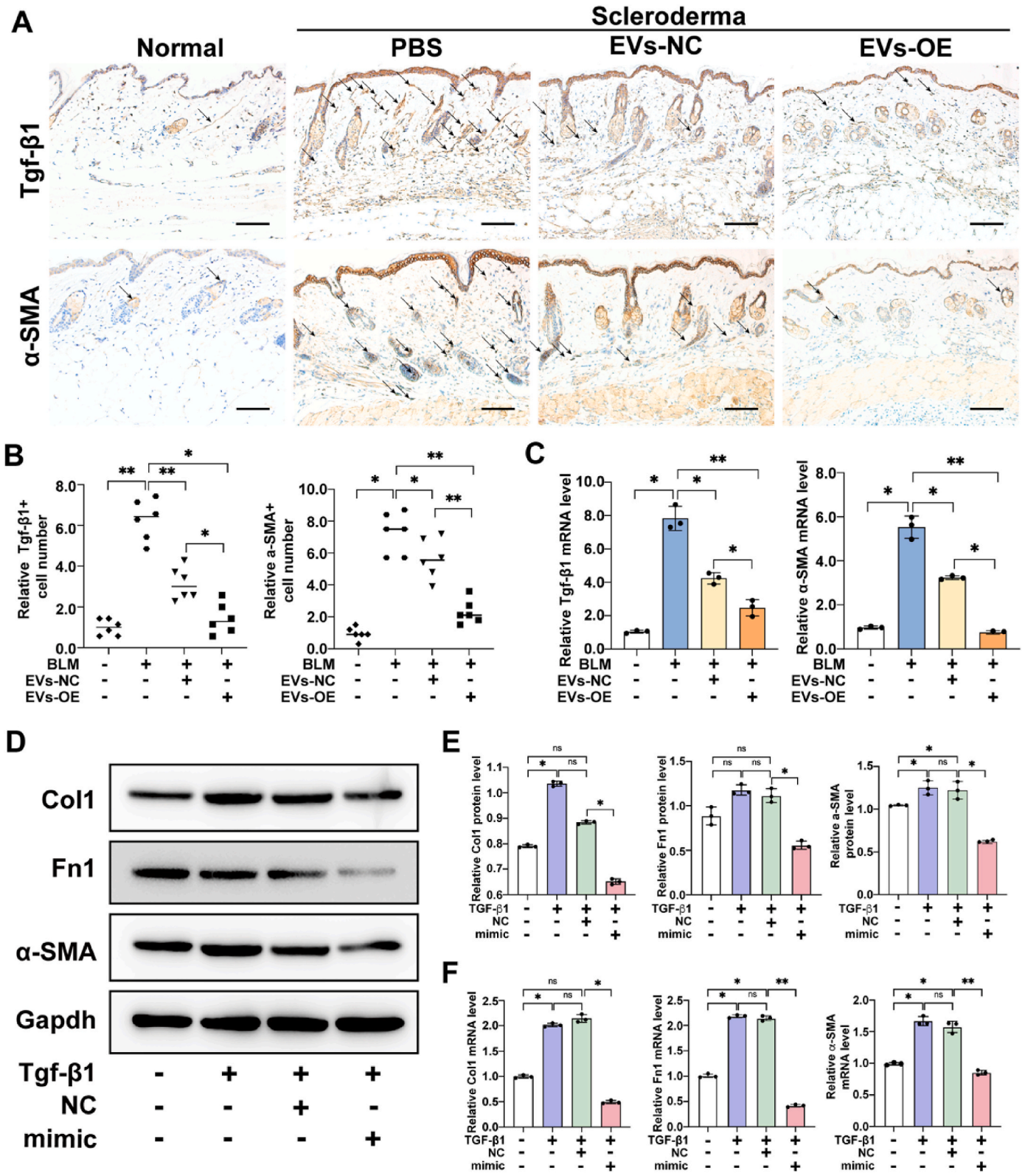

Fig. 6. miR-143-3p-modified EVs treatment inhibits fibroblast differentiation into myofibroblasts in mouse LoSc model.
(A) The expression of Tgf-β1 and α-SMA in the fibroblasts of the dermis was detected by IHC staining. Scale bar 200 μm. **(B)** Quantitative analysis of Tgf-β1 or α-SMA-positive cells in the sections (n = 3). **(C)** The mRNA levels of *α-SMA* and *Tgf-β1* in the dermis were detected with RT-PCR (n = 3). **(D–E)** The expression of Col1, Fn1, and α-SMA was detected by Western blot and quantified by Image J software (n = 3). **(F)** The expression of *Col1*, *Fn1*, and *α-SMA* in the mouse fibroblast treated with Tgf-β1, miR-143-3p mimics, or a control was quantified by RT-PCR (n = 3). Data are presented as mean ± SD; *, $P < 0.05$; **, $P < 0.01$.

(Figs. S1A–D). These results showed that EVs-i-miR-143-3p treatment does not reverse dermal thickening or subcutaneous adipose layer thinning.

Furthermore, we examine whether EVs-OE-miR-143-3p exert a more powerful anti-fibrosis effect on the BLM-induced LoSc mouse model than normal EVs. Two weeks after the subcutaneous injection of BMSC-EVs (EVs-NC or EVs-OE) treatments, compared to the normal mouse skin, PBS-treated mice showed that the dermis layer had significant thickening ($P = 0.0003$), the subcutaneous adipose layer was almost nonexistent, and the dermal architecture was disrupted (Fig. 5A). Both EVs-NC ($P = 0.0005$) and EVs-OE-miR-143-3p ($P = 0.0004$) can decrease the thickened dermis layer, and EVs with miR-143-3p-reinforced exert a better therapeutic effect than EVs-mir-NC ($P = 0.004$) (Fig. 5C and D).

Overall, these results revealed that miR-143-3p-modified EVs exerted a more powerful effect than EVs-mir-NC and that miR-143-3p strengthened the capability of EVs to improve BLM-induced dermal damage and fibrosis.

3.6. miR-143-3p-reinforced EVs reduce abnormal deposition of ECM of the dermis in LoSc mice

The deposition of ECM in the dermis is considered an atypical characteristic of scleroderma. Masson's trichrome staining was used to determine whether miR-143-3p modified BMSC-EVs were able to regulate the accumulation of excessive ECM components. As shown in Fig. 5B, BLM-induced LoSc skin showed an abundance of collagen and a dense ECM structure in the dermis, but both EVs-NC and EVs-OE-mir-143-3p greatly reduced ECM deposition. And EVs-OE-mir-143-3p exerted a better effect than EVs- NC. Consistently, the EVs-NC ($P = 0.0123$) and EVs-OE-mir-143-3p ($P = 0.0058$) treatments significantly reduced the hydroxyproline content, which was enhanced in the BLM induced mouse model, and the EVs-OE-mir-143-3p group had an even lower hydroxyproline content than the EVs-NC group ($P = 0.0278$) (Fig. 5E). Furthermore, *Col1* ($P = 0.0328$), *Col3* ($P = 0.0078$), and *Fn1* ($P = 0.0245$) mRNA expression levels were greatly increased in PBS-treated LoSc mice but were significantly decreased in mice treated with either EVs-NC ($P = 0.0267$) or EVs-OE-mir-143-3p ($P = 0.0318$). Additionally, EVs-OE-mir-143-3p treatment had a stronger impact than EVs-NC ($P = 0.0159$) (Fig. 5F).

For the inhibition of miR-143-3p of BMSC-EVs, the ECM and collagen of EVs-i-miR-143-3p were significantly higher than the EVs-NC treated tissues and similar to the PBS treated tissues (Figs. S1E–G). In addition, the expression of Fn1 was not improved in the EVs-i-miR-143-3p group compared to the control group. EVs-i-miR-143-3p greatly enhanced the expression of *Fn1* compared with that in the EVs-NC group ($P = 0.0251$).

The balance of matrix metalloproteinases (MMPs) and tissue inhibitor of metalloproteinase (TIMPs) is essential in maintaining collagen homeostasis. The imbalance between these two proteins leads to ECM and collagen deposition, and ultimately skin fibrosis [33,34]. As shown in Fig. 5G, the expression of MMP1 ($P = 0.0319$), MMP2 ($P = 0.0158$), TIMP1 ($P = 0.0219$), and TIMP2 ($P = 0.0317$) increased in the PBS-treated group compared with the normal group, but both EVs-NC and EVs-OE-mir-143-3p greatly reduced the levels of MMP1 ($P = 0.0109$), MMP2 ($P = 0.0158$), TIMP1 ($P = 0.0225$), and TIMP2 ($P = 0.0106$). And EVs-mir-143-3p showed a stronger ability to reduce the expression of MMP1 ($P = 0.0356$), MMP2 ($P = 0.0145$), TIMP1 ($P = 0.0238$), and TIMP2 ($P = 0.0219$). Consistent with immunohistochemical staining, the mRNA levels of the groups showed similar trends (Fig. 5H). Moreover, the ratio of MMP1/TIMP1 ($P = 0.0265$) and MMP2/TIMP2 ($P = 0.0264$) decreased in the PBS treated group compared with the normal group. EVs-OE-miR-143-3p showed an even stronger ability to enhance the ratio of MMP1/TIMP1 ($P = 0.0195$) and MMP2/TIMP2 ($P = 0.0313$), suggesting higher matrix remodeling activity.

Taken together, these results revealed that miR-143-3p-reinforced BMSC-EVs exerted more powerful effects by decreasing BLM-induced abnormal deposition of ECM and collagen density and improving cutaneous structural remodeling than normal BMSC-EVs.

3.7. miR-143-3p-reinforced EVs treatment inhibits fibroblast differentiation into myofibroblasts

Fibroblast activation and fibroblast-to-myofibroblast differentiation with TGFβ signaling pathway activation are typical features in the development of BLM-induced fibrosis in mouse LoSc models. In the mouse model, the number of Tgf-β1-positive cells was significantly decreased in the EVs-NC groups compared to the PBS-treated ($P = 0.0053$) but similar in the EVs-i-miR-143-3p and PBS-treated groups ($P = 0.0871$) (Figs. S2A and C). Similar observations were obtained by RT-PCR analysis of *Tgf-β1* mRNA expression (Figure S2E). In addition, the expression of α-SMA was also examined. As shown in Figs. S2B and D, EVs-i-miR-143-3p did not decrease the number of α-SMA-positive cells, in contrast to EVs-NC. And the results of RT-PCR were consistent with those of immunohistochemistry observations (Figure S2F).

We further examined whether miR-143-3p overexpression could further enhance the ability of BMSC-EVs to inhibit fibroblast differentiation into myofibroblasts *in vivo*. As shown in Fig. 6A and B, there was significantly more accumulation of Tgf-β1-positive cells in the dermis layer in the LoSc mice than in the normal mice ($P = 0.0058$), but both EVs-mir-NC ($P = 0.0078$) and EVs-mir-143-3p ($P = 0.0211$) greatly reduced the number of TGF-β1-positive cells. And EVs-mir-143-3p showed an even stronger ability to reduce Tgf-β1-positive cells. In addition, the number of α-SMA + myofibroblasts was significantly enhanced in the BLM treated mice ($P = 0.0376$), but decreased in both the EVs-mir-NC ($P = 0.0276$) and EVs-mir-143-3p ($P = 0.0072$) treatment groups. The EVs-OE-mir-143-3p group showed fewer α-SMA + myofibroblasts than the EVs-NC groups ($P = 0.0063$). Consistent with immunohistochemical staining, the mRNA expression of Tgf-β1 and α-SMA in the BLM induced mouse model was significantly higher than that in normal mice and was reduced after EVs-NC or EVs-OE-mir-143-3p treatment (Fig. 6C). In this experiment, EVs-OE-mir-143-3p performed better than EVs-NC.

These results demonstrated that subcutaneous injection of miR-143-3p-reinforced EVs exerted powerful effects by preventing myofibroblast formation in the dermis. These results suggested that miR-143-3p played a key role in BMSC-EVs inhibiting fibroblast differentiation into myofibroblasts.

3.8. miR-143-3p agomir treatment inhibits differentiation of fibroblasts to myofibroblasts and abnormal deposition of collagen in the LoSc model

The above results suggested that miR-143-3p might be a promising therapeutic target for the treatment of patients with scleroderma. We therefore sought to validate the therapeutic effect of miR-143-3p *in vivo*. miR-143-4p agomir-treated mice showed thinner dermal layer thickness ($P = 0.0218$) and a thicker subcutaneous adipose layer ($P = 0.0124$) than those of the agomir-NC group. In addition, compared with the agomir-NC group, miR-143-4p agomir improved the dermal architecture of mice (Figs. S3A, C, and D). miR-143-4p agomir significantly decreased ECM deposition compared with that in the agomir-NC group (Figure S3B). Consistently, miR-143-4p agomir suppressed the expression of the fibrotic markers Col1 ($P = 0.0127$) and Fn1 ($P = 0.0226$) (Figure S3E). RT-PCR also confirmed these observations by detecting fibrosis-related markers. These findings were further supported by RT-PCR that identified fibrosis-related markers (Fig. S3F). These results revealed that miR-143-3p can improve BLM-induced dermal fibrosis and damage.

Furthermore, we evaluated the expression of key fibrotic factors, including Tgf-β1 and α-SMA. As shown in Figs. S4A–B, miR-143-3p agomir greatly reduced the number of Tgf-β1-positive cells ($P = 0.0302$) and α-SMA-positive myofibroblasts ($P = 0.0187$) in the dermis

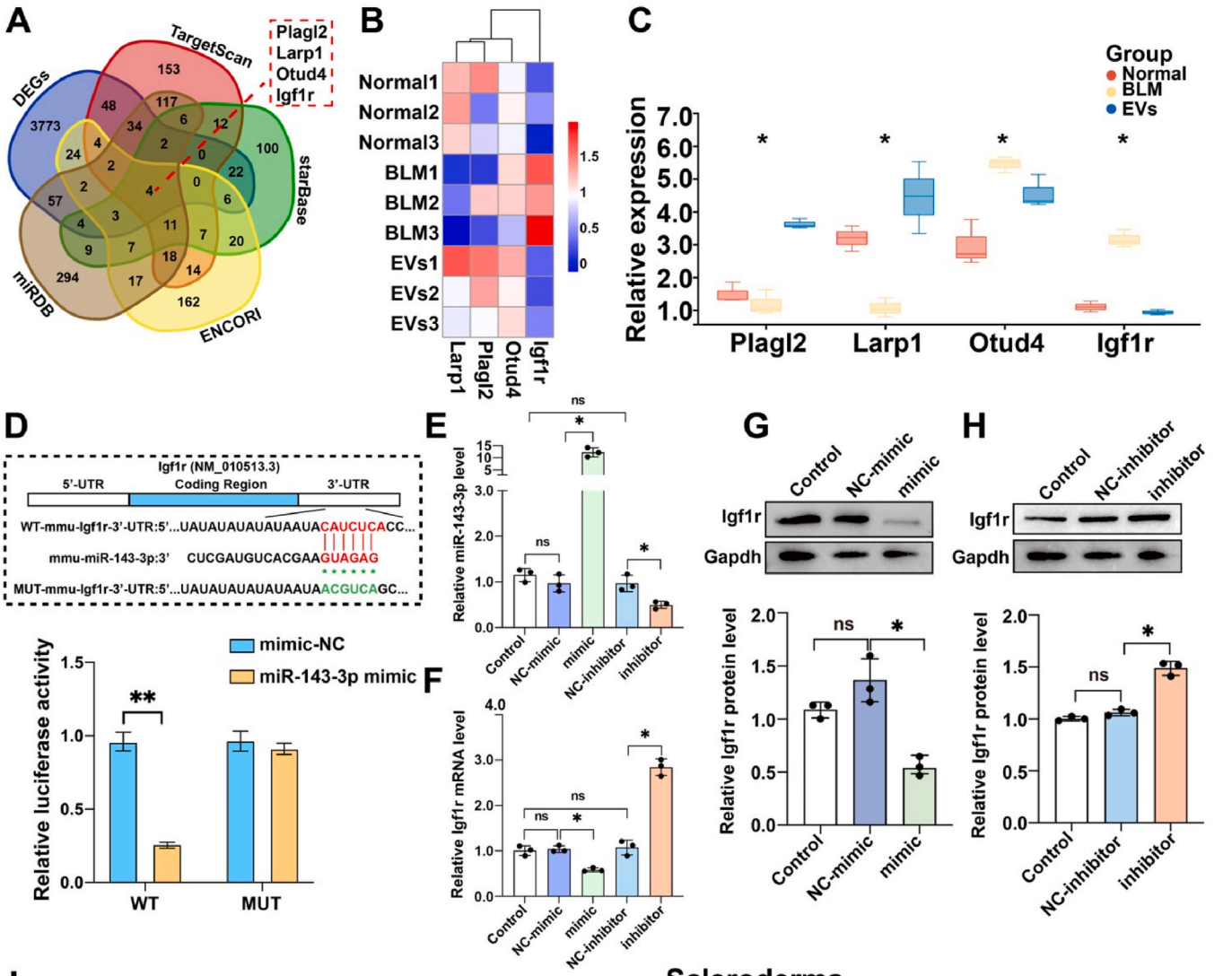

(caption on next page)

Fig. 7. miR-143-3p inhibits *Igf1r* by targeting the mRNA 3′-UTR of *Igf1r*.
(A) Candidate target genes of miR-143-3p were predicted by intersecting outputs from four online databases (TargetScan, miRTarBase, ENCORI, and microRNA.org) and DEGs of mouse LoSc skin tissues treated with BMSC-EVs. **(B–C)** The heatmap and violin plot showed the expression of the 4 hub genes in the mouse LoSc model treated with BMSC-EVs or control ($P < 0.05$; $n = 3$). **(D)** Luciferase reporter assays of HEK293 cells with transfection of WT/MUT-psiCHECK-Igf1r along with miR-143-3p mimic or NC-mimic as indicated to confirm the interaction of miR-143-3p and *Igfr1r* ($n = 6$). **(E–F)** The expression of miR-143-3p (E) and *Igf1r* (F) in the fibroblasts treated with miR-143-3p mimics or inhibitors was detected by RT-PCR ($n = 3$). **(G–H) The** protein level of Igf1r in the mouse fibroblasts treated with miR-143-3p mimics or inhibitors was detected by Western blot ($n = 3$). **(I)** Representative immunohistochemical staining shows the localization of Igf1r in skin tissues of mouse LoSc with miR-143-3p reinforced BMSC-EVs treatment. Scale bar: 200 μm. **(J)** Quantitative analysis of the Igf1r positive cells in the mouse skin tissues ($n = 3$). **(K)** The expression of *Igf1r* in the skin tissue was detected by RT-PCR ($n = 3$). **(L–M)** Relative expression levels of Igf1r protein in mouse skin tissues ($n = 3$). Data are presented as mean ± SD; *, $P < 0.05$; **, $P < 0.01$.

layer compared with that in the agomir-NC group. The mRNA expression of Tgf-β1 and α-SMA is consistent with immunohistochemical staining results (Figure S4 C). These results revealed that miR-143-3p suppressed fibroblast differentiation into myofibroblasts by decreasing the expression of Tgf-β1 in the dermis and validated the therapeutic benefits of miR-143-3p-reinforced.

3.9. miR-143-3p target the mRNA 3′-UTR of IGF1R

To gain insight into the potential target and mechanism of miR-143-3p of the BMSC-EVs regulation of fibrosis in fibroblasts, high-throughput RNA-seq was applied to analyze the skin tissues of LoSc mice with or without BMSC-EVs treatment. The DEGs of the two groups were screened as a dataset for potential targeting genes of BMSC-EVs (Fold-Change ≥1.2, $P < 0.05$) (GSE165117). Additionally, four public databases (including TargetScan, miRDB, starBase, and ENCORI) for target gene prediction of miRNAs were applied to efficiently screen the possible targets of miR-143-3p. Four target genes were identified from the intersection of four online databases and DEGs, including *Igf1r*, *Larp1*, *Otud4*, and *Plagl2* (Fig. 7A). And the relative expression of the four genes in the mouse LoSc skin tissues, which were treated with the BMSC-EVs or a control, is shown in Fig. 7B. The levels of Igf1r that had been elevated in the BLM-induced LoSc model were considerably reduced after BMSC-EVs treatment ($P = 0.0387$) (Fig. 7C). Therefore, we infer that Igf1r may be a key target of miR-143-3p mediated regulation of fibrosis in scleroderma.

We further applied the dual-luciferase reporter gene assay to confirm the interaction of miR-143-3p and Igf1r. Firstly, the presence of a binding site (3′-UTR of Igf1r) for miR-143-3p in the Igf1r gene was predicted with TargetScan (Fig. 7D). According to binding-site prediction, we generated wild-type (WT) and mutant (MUT) mRNA of Igf1r in the 3′-UTR sequences containing the binding site of miR-143-3p. The luciferase activity of wild-type sequences was markedly decreased by co-transfection with miR-143-3p mimics ($P = 0.0062$), but there was almost no change in the mutant sequence, suggesting that the 3′-UTR of Igf1r mRNA is a binding site and target of miR-143-3p.

Next, we evaluated whether miR-143-3p moderates the protein and mRNA expression of Igf1r in mouse skin fibroblasts upon transfection with miR-143-3p mimics or inhibitors. The protein ($P = 0.0162$) and mRNA ($P = 0.0381$) expression of Igf1r were significantly decreased after miR-143-3p mimic transfection (Fig. 7E–G). By contrast, inhibitors were transfected into the mouse skin fibroblast to reduce the level of miR-143-3p, and the mRNA ($P = 0.0372$) and protein ($P = 0.0264$) levels of Igf1r were found to be increased (Fig. 7F and H). These results show that miR-143-3p binds to the 3′-UTR of Igf1r to inhibit the expression of *Igf1r*.

We also confirmed the expression of Igf1r in the mouse LoSc model with miR-143-3p reinforced BMSC-EVs or BMSC-EVs treatments. The expression of Igf1r and the Igf1r-positive cells in the mouse dermis was downregulated compared with that in the normal and control (EVs-miR-NC) groups (Fig. 7I–K). The level of Igf1r in mRNA and protein of the dermis was also consistent with that of immunohistochemistry by Western blot and RT-PCR (Fig. 7L and M). Taken together, these data determined that miR-143-3p of BMSC-EVs targeted the Igf1r of fibroblasts of the dermis to decrease the level of Igf1r in the LoSc mouse model.

3.10. miR-143-3p-modifed EVs alleviate skin fibrosis by targeting IGF1-IGF1R

We further study the potential mechanism of IGF1R inhibition in the development and treatment of scleroderma. The public RNA sequencing datasets, which include 10 normal tissues and 28 LoSc tissues, were first involved in this study [28,29]. The expression of IGF1R in the skin of LoSc patients significantly increased compared to the normal skin ($P = 0.0094$) (Fig. 8A). In line with this analysis, the expression of IGF1R in the skin tissues of LoSc patients involved in our study was increased compared to normal skin tissues (Fig. 8B). There was also a significant rise in the level of *IGF1R* mRNA in the LoSc skin tissues ($P = 0.0285$, $n = 4$) (Fig. 8C).

We further analyzed the single-cell sequencing datasets (GSE195452), which include 56 healthy controls and 97 LoSc patients at different stages of LoSc [24]. The cell types include fibroblast cell, pericyte cell, epithelial cell, endothelial cell, T cell, myeloid cell, B cell, and mast cell, were revealed with a UMAP plot (Fig. 8D). The markers of these cell types were shown in Fig. 8E, and the fibroblasts were featured with DCN and COL1A1 (Fig. 8E). Then, the fibroblast cells were sub-clustered into 13 clusters with UMAP (Fig. 8F). Interestingly, the Fib_11 (sub-cluster 11 of fibroblast) clusters show a high proportion in the early stages (Fig. 8G). And Fib_11 clusters expressed the IGF1, IGFBP4, IGFBP7, FOS, and ACTA2 (α-SMA) (Fig. 8H). The distribution of *IGF1* and *IGF1R* in the 13 sub-clusters of fibroblasts during the 4 stages was shown in Fig. 8I. In the early stage, *IGF1* was relatively high enrichment in Fib_11. And the IGF1R positive cells were distributed in all sub-clusters of fibroblasts. GO analysis of the feature genes of Fib_11 reveals that the Fib_11 cluster is characterized by cell activation, MAPK cascade, intracellular cytoskeleton organization, etc. (Fig. 8J). Thus, we consider that IGF1-IGF1R have an important role in fibroblast activation to promote the development of scleroderma.

3.11. miR-143-3p-modifed EVs alleviate skin fibrosis by targeting IGF1R/MAPK pathway of dermis

The activated myofibroblasts were from the fibroblast and epithelial cells with an endothelial-to-mesenchymal transition. In Fig. 8B, the epidermis layer was also positive for IGF1R staining compared to the control tissues of LoSc patients. Thus, we analyze the epithelial cell cluster of Fig. 8D of the single-cell RNA sequencing datasets. The epithelial cells were subclustered into 11 clusters (Fig. 9A). The IGF1R-positive cells were highly enriched in the cluster 3 (Fig. 9B and C). GO analysis of the feature genes of Epi_3 reveals that the Epi_3 cluster is characterized by MAPK cascade, epithelial to mesenchymal transition, epithelial cell proliferation, etc. (Fig. 9D). The Fib_11 from fibroblasts and Epi_3 from epithelial cells show stronger interactions based on the IGF signaling pathway (Fig. 9E). Moreover, the pairs of ligand-receptor analyzed confirmed that the Fib_11 from and Epi_3 were relative to the IGF1-IGF1R function and showed the role of IGF1R in the epidermis of the skin (Fig. 9F).

The IGF1/IGF1R signaling pathway was reported to regulate cell growth and differentiation by the AKT/MAPK signaling pathway.

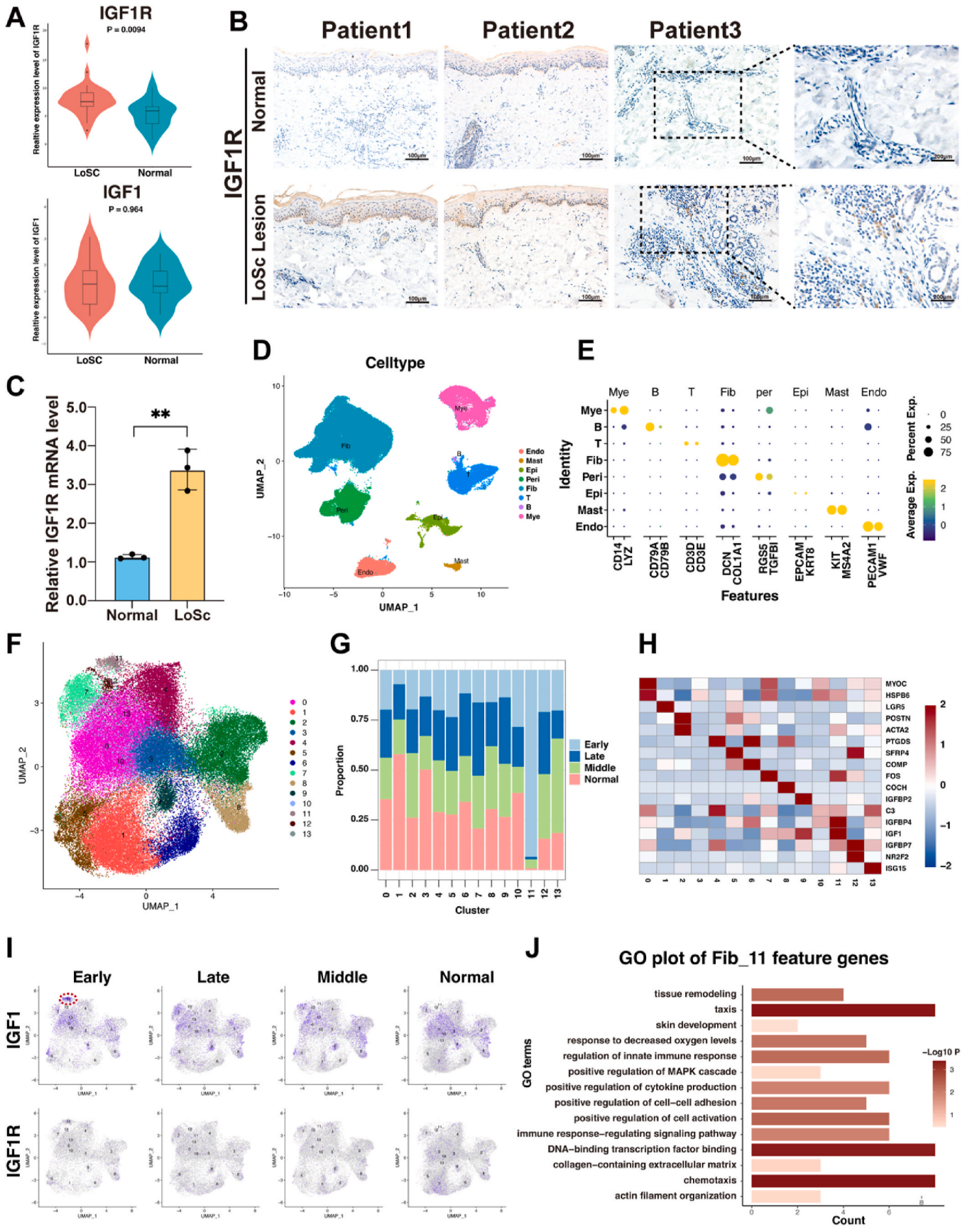

(caption on next page)

Fig. 8. The highly expression of IGF1R in fibroblast of LoSc patients.
(A) The expression of *IGF1* and *IGF1R* in the skin of LoSc patients based on the RNA sequencing dataset from GSE166861 and GSE166863. IGF1R: Log2FC = 2.586155914; P value = 0.0094. **(B)** Representative IHC staining of IGF1R in representative skin sections of normal and lesion skin samples from LoSc patients. Scale bar: 100 μm. **(C)** Quantification of *IGF1R* in human skin tissues with LoSc by RT-PCR. **(D)** The UMAP plot showed cell types in the skin of LoSc patients and normals based on the single cell RNA sequencing dataset from GSE195452. **(E)** Markers labeling cell types in the UMAP plot. Cell types: Fib indicates fibroblast cell; Peri indicates pericyte cell; Epi indicates epithelial cell; Endo indicates endothelial cell. T indicates T cell; Mye indicates myeloid cell; B indicates B cell. Mast indicates mast cell. **(F)** The UMAP plot showed clusters of fibroblast cells in Figure D. **(G)** The proportion of different stages of LoSc disease in fibroblast clusters. **(H)** The feature genes in each cluster of fibroblasts. **(I)** The expressions of *IGF1* and *IGF1R* in fibroblast cells from different stages of LoSc patients and normal controls. **(J)** The GO plot shows the characteristic genes of the Fib_11 cluster.

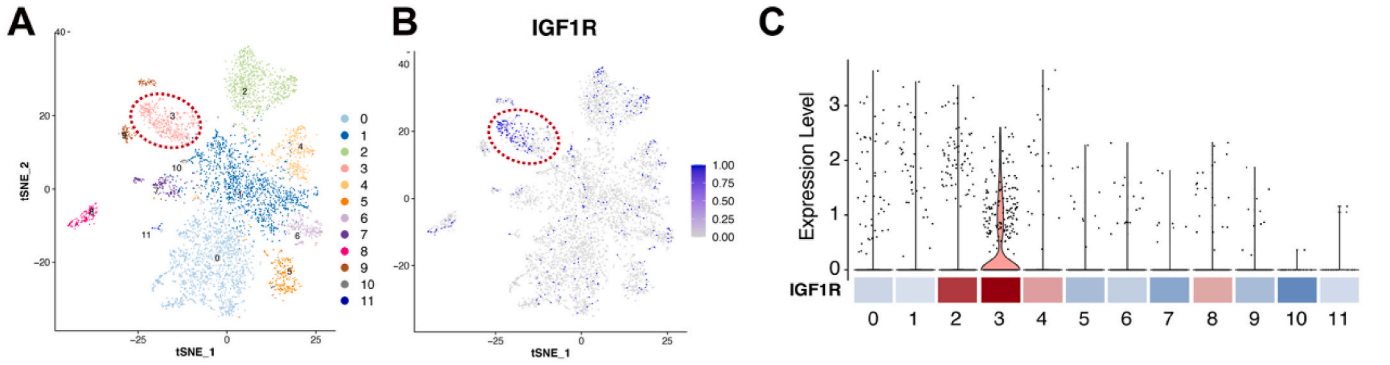

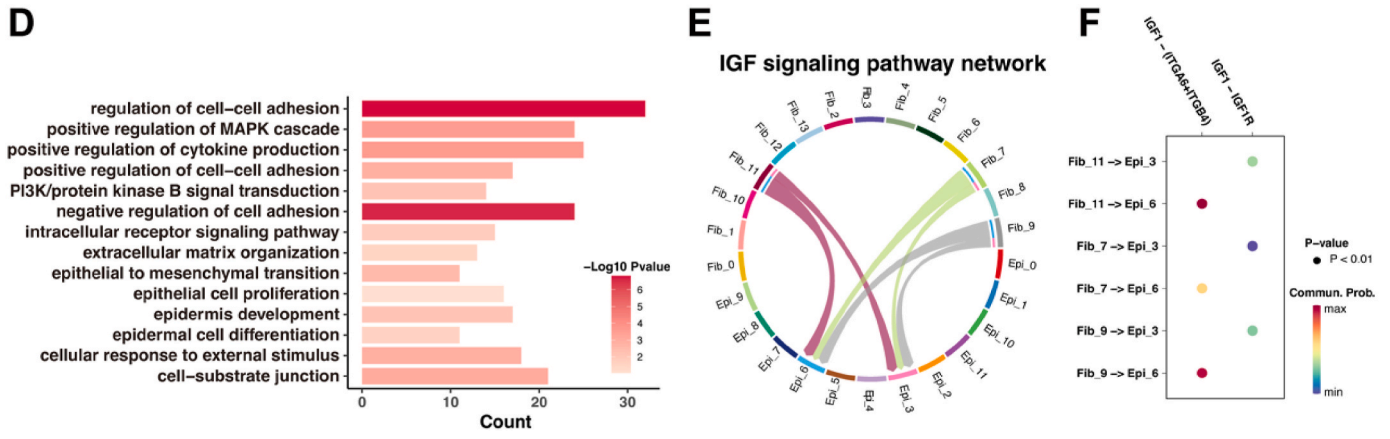

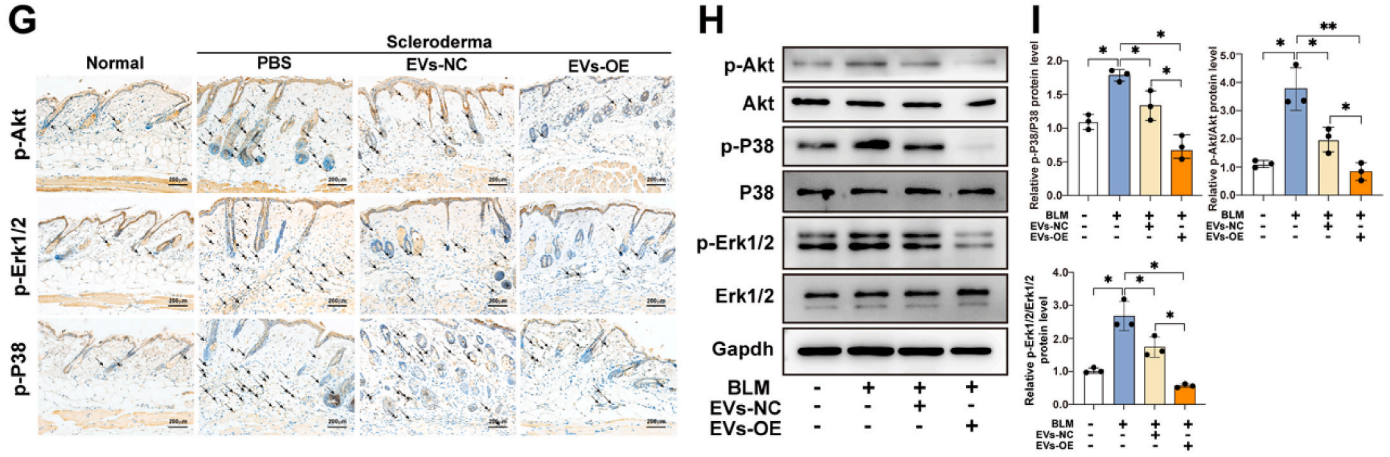

Fig. 9. miR-143-3p inhibits IGF1R-AKT/MAPK pathway.
(A) The UMAP plot showed clusters of epithelial cells in the skins of LoSc patients and normal controls. **(B)** The expression of IGF1R in epithelial cells from LoSc patients and normal controls. **(C)** The expression of IGF1R in each cluster of epithelial cells. **(D)** The GO plot shows the characteristic genes of the Epi_3 cluster. **(E)** The chord diagram showed the interactions in the IGF signaling pathway between all clusters of fibroblast and epithelial cells. **(F)** The pairs of ligand-receptors in the IGF signaling pathway between clusters of fibroblast and epithelial cells. **(G)** Representative immunohistochemical staining of phospho-AKT, phospho-ERK1/2, and phospho-P38. **(H–I)** The expression and phosphorylation levels of AKT, ERK1/2, and P38 in the BMSC-EVs treated skin tissues in the mouse LoSc model (n = 3). Data are presented as mean ± SD; *, P < 0.05; **, P < 0.01.

Analysis of the mouse LoSc tissues treated with BMSC-EVs by immunohistochemistry assays revealed that the BLM treatment enhanced the relative levels of phosphorylated AKT, phosphorylated ERK1/2, and phosphorylated P38 (Fig. 9G). These phosphorylations of AKT, ERK1/2, and P38 were partially inhibited by the administration of BMSC-EVs and, in greater part, blocked by the miR-143-3p reinforced BMSC-EVs (Fig. 9H and I). In conclusion, these results demonstrated that miR-143-3p-reinforced EVs attenuated the activation of AKT/MAPK signaling pathways via inhibiting the IGF1-IGF1R pathway in dermal fibrosis.

4. Discussion

Localized scleroderma (LoSc), featuring excessive fibrosis of skin, remains a formidable clinical challenge and has limited therapeutic options [35,36]. The mice induced with subcutaneous injection of BLM were used as skin disease models of LoSc because the pathological changes in dermis, such as greater dermal thickness and collagen buildup, are comparable to those seen in LoSc patients [37]. Previously, we reported that the BMSC-EVs can treat the skin thickening and deposition of ECM in the BLM induced mouse LoSc model. In addition, Chen et al. also indicated that treatment with BMSC-EVs restores the osteopenic phenotype of tight-skin mutant mice scleroderma model through the transmission of miR-151-5p [38]. miRNAs of BMSC-EVs, which inhibit myofibroblast formation by downregulating the expression of TGF-β1 in the dermis, are believed to be important in their therapeutic effect on LoSc [39]. In the present study, miR-21a-5p supplementation shows no treatment on the LoSc model, which is consistent with the report that miR-21a-5p inhibition can alleviate systemic sclerosis by targeting STAT3 signaling by Jin-Sil Park et al. recently [40]. Here, we present miR-143-3p, a highly abundant miRNA of the mouse BMSC-EVs, which plays a key role in the therapeutic effects of the BMSC-EVs on dermis fibrosis and skin structural remodeling in the mouse LoSc model.

The surface protein CD47 enables EVs to evade the mononuclear phagocytic system. Furthermore, EVs can efficiently transfer nucleic acids across biological barriers to target cells [14]. Engineering MSCs with specific enriched miRNAs can enhance the functional effects of their EVs on target cells and organs. For instance, miR-29a-3p-modified exosomes derived from umbilical cord stem cells have been shown to promote tendon repair [41]. Similarly, engineered ADSCs can deliver miR-181-5p to damaged liver cells, effectively attenuating liver fibrosis [42]. Our study indicated that miR-143-3p of BMSC-EVs can be transported into fibroblasts and significantly inhibited myofibroblast formation and synthesis of collagen. Even though upregulation of miR-143-3p reported to be associated with fibrosis and abnormal ECM metabolic pathological processes in the organs, including the heart and cornea [43,44]. However, in the fibroblast of the skin, increasing miR-143-3p can prevent hypertrophic scarring by reducing ECM production-associated protein expression by targeting CTGF [45,46]. These reports were consistent with our findings in the skin of LoSc. We demonstrated that the supplementation of miR-143-3p with EVs or agomir can improve the dermis structure and status, including the deposition of ECM, in the dermis of the LoSc model.

IGF1 integrates with IGF1R, a type 2 tyrosine kinase transmembrane receptor, to activate the epithelial-mesenchymal transition of epithelial cells and the proliferation and differentiation of fibroblasts into myofibroblasts and increases synthesis of collagen and extracellular matrix in myofibroblasts [47–50]. Blockade of the IGF1/IGF1R pathway by an IGF1R antibody induces fibroblast apoptosis and subsequent resolution of pulmonary fibrosis [47,48]. Regulation of myofibroblast differentiation in human embryonic lung fibroblasts through modulating ERK1/2 and p38 pathways, and these signal pathways may therefore represent an attractive treatment modality in pulmonary fibrosis [51]. Reinforced miR-143-3p attenuated ECM protein deposition and reduced the expression of type I collagen and fibronectin in airway smooth muscle cells [52]. We raised IGF1R as a target in miR-143-3p-mediated regulation of fibrosis and ECM protein deposition in the dermis. And IGF1R activation by IGFBPs plays a pathogenic role in the development of autoimmune diseases [53]. miR-143-3p-reinforced EVs improve BLM-induced dermal damage and abnormalities by inhibiting IGF1R expression and disrupting IGF1R-mediated AKT/MAPK signaling pathways. Bleomycin induction activates the AKT and MAPK signaling pathways of dermal fibroblasts. miR-143-3p-reinforced EVs improved skin fibrosis and tissue remodeling via the modulation of the AKT/MAPK signaling pathway by targeting IGF1R. As an autoimmune disease, LoSc involves a complex interplay of multiple biological and physiological factors in its onset and progression. Similarly, BMSC-EVs are rich in diverse nucleic acids and proteins with essential cellular functions. Therefore, we propose that the miR-143-3p-IGF1R axis plays a pivotal role in BMSC-EV-based treatment for LoSc. Moreover, miR-143-3p-modified EVs warrant further investigation in the context of the IGF1-IGF1R axis, supported by additional evidence.

In conclusion, miR-143-3p mediates the therapeutic effect of BMSC-EVs in LoSc. miR-143-3p is important in regulating various cellular processes and balancing numerous factors whose expression is altered in LoSc. miR-143-3p-reinforced EVs exerted a more powerful effect than normal EVs to inhibit dermal fibrosis and improve skin tissue remodeling. These effects were mainly obtained via the modulation of the AKT/MAPK signaling pathway by targeting IGF1R. In the future, the pharmacology and toxicology of the EVs deserve further investigation to promote the application of BMSC-EVs in the clinical treatment of LoSc.

CRediT authorship contribution statement

Jiahui Jin: Writing – original draft, Resources, Project administration, Methodology, Investigation, Formal analysis, Data curation, Conceptualization. **Zhe Wang:** Validation, Software, Resources, Methodology, Investigation, Funding acquisition, Formal analysis, Data curation. **Yifan Liu:** Formal analysis, Data curation. **Jie Chen:** Methodology, Investigation. **Miao Jiang:** Project administration, Methodology. **Lixia Lu:** Software, Resources. **Jingying Xu:** Methodology, Funding acquisition. **Furong Gao:** Validation, Supervision, Resources, Methodology. **Juan Wang:** Resources, Project administration. **Jieping Zhang:** Project administration, Methodology. **Guo-Tong Xu:** Writing – review & editing, Funding acquisition, Conceptualization. **Caixia Jin:** Writing – review & editing, Methodology, Funding acquisition, Formal analysis, Data curation, Conceptualization. **Haibin Tian:** Writing – review & editing, Supervision, Methodology, Funding acquisition, Formal analysis, Conceptualization. **Jingjun Zhao:** Methodology, Investigation. **Qingjian Ou:** Writing – review & editing, Writing – original draft, Supervision, Methodology, Investigation, Funding acquisition, Formal analysis, Data curation, Conceptualization.

Declaration of competing interest

The authors declare that they have no known competing financial interests or personal relationships that could have appeared to influence the work reported in this paper.

Acknowledgements

This study was supported by the National Natural Science Foundation of China (82373482, 82404124, 82271108, 81372071), the Shanghai Municipal Health Commission (20234Y0113), the Shanghai Sailing Program (23YF1457700), and the Fundamental Research Funds for the Central Universities (22120220621).

Appendix A. Supplementary data

Supplementary data to this article can be found online at https://doi.org/10.1016/j.jaut.2025.103422.

Data availability

Data will be made available on request.

References

[1] D.A. Gyftaki-Venieri, D.J. Abraham, M. Ponticos, Insights into myofibroblasts and their activation in scleroderma: opportunities for therapy? Curr. Opin. Rheumatol. 30 (2018) 581–587.
[2] A. Gorkiewicz-Petkow, A. Kalinska-Bienias, Systemic involvement in localized scleroderma/morphea, Clin. Dermatol. 33 (2015) 556–562.
[3] S. Christen-Zaech, M.D. Hakim, F.S. Afsar, A.S. Paller, Pediatric morphea (localized scleroderma): review of 136 patients, J. Am. Acad. Dermatol. 59 (2008) 385–396.
[4] L. Abbas, A. Joseph, E. Kunzler, H.T. Jacobe, Morphea: progress to date and the road ahead, Ann. Transl. Med. 9 (2021) 437.
[5] C. Yan, W.A. Grimm, W.L. Garner, L. Qin, T. Travis, N. Tan, et al., Epithelial to mesenchymal transition in human skin wound healing is induced by tumor necrosis factor-alpha through bone morphogenic protein-2, Am. J. Pathol. 176 (2010) 2247–2258.
[6] H.E. Talbott, S. Mascharak, M. Griffin, D.C. Wan, M.T. Longaker, Wound healing, fibroblast heterogeneity, and fibrosis, Cell Stem Cell 29 (2022) 1161–1180.
[7] R. Schuster, F. Younesi, M. Ezzo, B. Hinz, The role of myofibroblasts in physiological and pathological tissue repair, Cold Spring Harbor Perspect. Biol. 15 (2023).
[8] P. Pakshir, B. Hinz, The big five in fibrosis: macrophages, myofibroblasts, matrix, mechanics, and miscommunication, Matrix Biol. 68–69 (2018) 81–93.
[9] C.P. Denton, D. Khanna, Systemic sclerosis, Lancet 390 (2017) 1685–1699.
[10] B. Hinz, D. Lagares, Evasion of apoptosis by myofibroblasts: a hallmark of fibrotic diseases, Nat. Rev. Rheumatol. 16 (2020) 11–31.
[11] J.C. Broen, T.R. Radstake, M. Rossato, The role of genetics and epigenetics in the pathogenesis of systemic sclerosis, Nat. Rev. Rheumatol. 10 (2014) 671–681.
[12] S. Jafarinejad-Farsangi, A. Farazmand, F. Gharibdoost, E. Karimizadeh, F. Noorbakhsh, H. Faridani, et al., Inhibition of MicroRNA-21 induces apoptosis in dermal fibroblasts of patients with systemic sclerosis, Int. J. Dermatol. 55 (2016) 1259–1267.
[13] X. Deng, Y. Su, H. Wu, R. Wu, P. Zhang, Y. Dai, et al., The role of microRNAs in autoimmune diseases with skin involvement, Scand. J. Immunol. 81 (2015) 153–165.
[14] O.M. Elsharkasy, J.Z. Nordin, D.W. Hagey, O.G. de Jong, R.M. Schiffelers, S. E. Andaloussi, et al., Extracellular vesicles as drug delivery systems: why and how? Adv. Drug Deliv. Rev. 159 (2020) 332–343.
[15] H. Valadi, K. Ekström, A. Bossios, M. Sjöstrand, J.J. Lee, J.O. Lötvall, Exosome-mediated transfer of mRNAs and microRNAs is a novel mechanism of genetic exchange between cells, Nat. Cell Biol. 9 (2007) 654–659.
[16] Z. Shen, W. Huang, J. Liu, J. Tian, S. Wang, K. Rui, Effects of mesenchymal stem cell-derived exosomes on autoimmune diseases, Front. Immunol. 12 (2021) 749192.
[17] J.S. Rockel, R. Rabani, S. Viswanathan, Anti-fibrotic mechanisms of exogenously-expanded mesenchymal stromal cells for fibrotic diseases, Semin. Cell Dev. Biol. 101 (2020) 87–103.
[18] M. Jiang, Y. Yu, J. Luo, Q. Gao, L. Zhang, Q. Wang, et al., Bone marrow-derived mesenchymal stem cells expressing thioredoxin 1 attenuate bleomycin-induced skin fibrosis and oxidative stress in scleroderma, J. Invest. Dermatol. 137 (2017) 1223–1233.
[19] D.G. Phinney, M.F. Pittenger, Concise review: MSC-derived exosomes for cell-free therapy, Stem Cell. 35 (2017) 851–858.
[20] A. Hassanzadeh, H.S. Rahman, A. Markov, J.J. Endjun, A.O. Zekiy, M.S. Chartrand, et al., Mesenchymal stem/stromal cell-derived exosomes in regenerative medicine and cancer; overview of development, challenges, and opportunities, Stem Cell Res. Ther. 12 (2021) 297.
[21] F. van den Hoogen, D. Khanna, J. Fransen, S.R. Johnson, M. Baron, A. Tyndall, et al., Classification criteria for systemic sclerosis: an American College of Rheumatology/European League against Rheumatism collaborative initiative, Arthritis Rheum. 65 (2013) 2737–2747, 2013.
[22] T. Arkachaisri, S. Pino, Localized scleroderma severity index and global assessments: a pilot study of outcome instruments, J. Rheumatol. 35 (2008) 650–657.
[23] T. Arkachaisri, S. Vilaiyuk, S. Li, K.M. O'Neil, E. Pope, G.C. Higgins, et al., The localized scleroderma skin severity index and physician global assessment of disease activity: a work in progress toward development of localized scleroderma outcome measures, J. Rheumatol. 36 (2009) 2819–2829.
[24] C. Gur, S.Y. Wang, F. Sheban, M. Zada, B. Li, F. Kharouf, et al., LGR5 expressing skin fibroblasts define a major cellular hub perturbed in scleroderma, Cell 185 (2022) 1373–1388, e20.
[25] J. Jin, Q. Ou, Z. Wang, H. Tian, J.Y. Xu, F. Gao, et al., BMSC-derived extracellular vesicles intervened the pathogenic changes of scleroderma in mice through miRNAs, Stem Cell Res. Ther. 12 (2021) 327.
[26] S. Hu, Z. Wang, C. Jin, Q. Chen, Y. Fang, J. Jin, et al., Human amniotic epithelial cell-derived extracellular vesicles provide an extracellular matrix-based microenvironment for corneal injury repair, J. Tissue Eng. 13 (2022) 20417314221122123.
[27] T. Dull, R. Zufferey, M. Kelly, R.J. Mandel, M. Nguyen, D. Trono, et al., A third-generation lentivirus vector with a conditional packaging system, J. Virol. 72 (1998) 8463–8471.
[28] E. Mirizio, C. Liu, Q. Yan, J. Waltermire, R. Mandel, K.L. Schollaert, et al., Genetic signatures from RNA sequencing of pediatric localized scleroderma skin, Front Pediatr 9 (2021) 669116.
[29] C. Schutt, E. Mirizio, C. Salgado, M. Reyes-Mugica, X. Wang, W. Chen, et al., Transcriptomic evaluation of juvenile localized scleroderma skin with histologic and clinical correlation, Arthritis Rheumatol. 73 (2021) 1921–1930.
[30] M.E. Ritchie, B. Phipson, D. Wu, Y. Hu, C.W. Law, W. Shi, et al., Limma powers differential expression analyses for RNA-sequencing and microarray studies, Nucleic Acids Res. 43 (2015) e47.
[31] R.M. Laxer, F. Zulian, Localized scleroderma, Curr. Opin. Rheumatol. 18 (2006) 606–613.
[32] F.S. Younesi, D.O. Son, J. Firmino, B. Hinz, Myofibroblast markers and microscopy detection methods in cell culture and histology, Methods Mol. Biol. 2299 (2021) 17–47.
[33] T. Takeuchi, M. Hayashi, T. Tamita, Y. Nomura, N. Kojima, A. Mitani, et al., Discovery of aryloxyphenyl-heptapeptide hybrids as potent and selective matrix metalloproteinase-2 inhibitors for the treatment of idiopathic pulmonary fibrosis, J. Med. Chem. 65 (2022) 8493–8510.
[34] S. Hemmann, J. Graf, M. Roderfeld, E. Roeb, Expression of MMPs and TIMPs in liver fibrosis - a systematic review with special emphasis on anti-fibrotic strategies, J. Hepatol. 46 (2007) 955–975.
[35] M. Matucci-Cerinic, T. Krieg, L. Guillevin, B. Schwierin, D. Rosenberg, P. Cornelisse, et al., Elucidating the burden of recurrent and chronic digital ulcers in systemic sclerosis: long-term results from the DUO Registry, Ann. Rheum. Dis. 75 (2016) 1770–1776.
[36] L. Chauvelot, D. Gamondes, J. Berthiller, A. Nieves, S. Renard, J. Catella-Chatron, et al., Hemodynamic response to treatment and outcomes in pulmonary hypertension associated with interstitial lung disease versus pulmonary arterial hypertension in systemic sclerosis: data from a study identifying prognostic factors in pulmonary hypertension associated with interstitial lung disease, Arthritis Rheumatol. 73 (2021) 295–304.
[37] T. Yamamoto, S. Takagawa, I. Katayama, K. Yamazaki, Y. Hamazaki, H. Shinkai, et al., Animal model of sclerotic skin. I: local injections of bleomycin induce sclerotic skin mimicking scleroderma, J. Invest. Dermatol. 112 (1999) 456–462.
[38] C. Chen, D. Wang, A. Moshaverinia, D. Liu, X. Kou, W. Yu, et al., Mesenchymal stem cell transplantation in tight-skin mice identifies miR-151-5p as a therapeutic target for systemic sclerosis, Cell Res. 27 (2017) 559–577.
[39] Y.X. Xu, S.D. Pu, X. Li, Z.W. Yu, Y.T. Zhang, X.W. Tong, et al., Exosomal ncRNAs: novel therapeutic target and biomarker for diabetic complications, Pharmacol. Res. 178 (2022) 106135.
[40] J.S. Park, C. Kim, J. Choi, H.Y. Jeong, Y.M. Moon, H. Kang, et al., MicroRNA-21a-5p inhibition alleviates systemic sclerosis by targeting STAT3 signaling, J. Transl. Med. 22 (2024) 323.
[41] Z. Yao, J. Li, H. Xiong, H. Cui, J. Ning, S. Wang, et al., MicroRNA engineered umbilical cord stem cell-derived exosomes direct tendon regeneration by mTOR signaling, J. Nanobiotechnol. 19 (2021) 169.
[42] Y. Qu, Q. Zhang, X. Cai, F. Li, Z. Ma, M. Xu, et al., Exosomes derived from miR-181-5p-modified adipose-derived mesenchymal stem cells prevent liver fibrosis via autophagy activation, J. Cell Mol. Med. 21 (2017) 2491–2502.
[43] B. Yu, M. Yu, H. Zhang, D. Xie, W. Nie, K. Shi, Suppression of miR-143-3p contributes to the anti-fibrosis effect of atorvastatin on myocardial tissues via the modulation of Smad2 activity, Exp. Mol. Pathol. 112 (2020) 104346.
[44] L. Zhang, J. Gao, A. Gong, Y. Dong, X. Hao, X. Wang, et al., The long noncoding RNA LINC00963 inhibits corneal fibrosis scar formation by targeting miR-143-3p, DNA Cell Biol. 41 (2022) 400–409.
[45] S. Mu, B. Kang, W. Zeng, Y. Sun, F. Yang, MicroRNA-143-3p inhibits hyperplastic scar formation by targeting connective tissue growth factor CTGF/CCN2 via the Akt/mTOR pathway, Mol. Cell. Biochem. 416 (2016) 99–108.
[46] J. Wei, Z. Wang, C. Zhong, H. Ding, X. Wang, S. Lu, LncRNA MIR503HG promotes hypertrophic scar progression via miR-143-3p-mediated Smad3 expression, Wound Repair Regen. 29 (2021) 792–800.
[47] J.E. Choi, S.S. Lee, D.A. Sunde, I. Huizar, K.L. Haugk, V.J. Thannickal, et al., Insulin-like growth factor-I receptor blockade improves outcome in mouse model of lung injury, Am. J. Respir. Crit. Care Med. 179 (2009) 212–219.
[48] W. Baszanowska, M. Misiura, I. Oscilowska, J. Palka, W. Miltyk, Extracellular prolidase (PEPD) induces anabolic processes through EGFR, β(1)-integrin, and IGF-1R signaling pathways in an experimental model of wounded fibroblasts, Int. J. Mol. Sci. 22 (2021).
[49] N.K. Harrison, A.D. Cambrey, A.R. Myers, A.M. Southcott, C.M. Black, R.M. du Bois, et al., Insulin-like growth factor-I is partially responsible for fibroblast proliferation induced by bronchoalveolar lavage fluid from patients with systemic sclerosis, Clin. Sci. (Lond.) 86 (1994) 141–148.
[50] Y.M. Yan, J.N. Zheng, Y. Li, Q.R. Yang, W.Q. Shao, Q. Wang, Insulin-like growth factor binding protein 7 as a candidate biomarker for systemic sclerosis, Clin. Exp. Rheumatol. 39 (Suppl 131) (2021) 66–76.
[51] J. Weng, M. Tu, P. Wang, X. Zhou, C. Wang, X. Wan, et al., Amiodarone induces cell proliferation and myofibroblast differentiation via ERK1/2 and p38 MAPK signaling in fibroblasts, Biomed. Pharmacother. 115 (2019) 108889.
[52] W. Cheng, K. Yan, L.Y. Xie, F. Chen, H.C. Yu, Y.X. Huang, et al., MiR-143-3p controls TGF-beta1-induced cell proliferation and extracellular matrix production in airway smooth muscle via negative regulation of the nuclear factor of activated T cells 1, Mol. Immunol. 78 (2016) 133–139.
[53] R.C. Baxter, Signaling pathways of the insulin-like growth factor binding proteins, Endocr. Rev. 44 (2023) 753–778.